Tectonic tremor characterized by principal-component analysis in the vicinity of central Chile and Argentina

Nishitsuji, Yohei; Marín, Luis Franco ; Gomez, Martín; Rowe, C.A; Draganov, Deyan

DOI
10.1016/j.jsames.2019.04.022

Publication date
2019

Document Version
Accepted author manuscript

Published in
Journal of South American Earth Sciences

Tectonic Tremor Characterized by Principal-Component Analysis in the Vicinity of Central Chile and Argentina

Author's names: Yohei Nishitsuji[1,2*], Luis Enrique Franco Marin[3], Martín Gomez[4], Charlotte Rowe[5], Deyan Draganov[1]

Affiliation: [1]Department of Geoscience and Engineering,
Delft University of Technology, The Netherlands
[2]Petro Summit E&P Corporation, Japan
[3]OVDAS-SERNAGEOMIN, Chile
[4]ICES, CNEA, Argentina
[5]Earth and Environmental Sciences Division,
Los Alamos National Laboratory, USA

Date of submission: 14-Aug, 2018

Corresponding author:
name : Yohei Nishitsuji
address: Department of Geoscience and Engineering,
Delft University of Technology
Stevinweg 1, 2628 CN Delft, Netherlands
P.O. Box 5048, 2600 GA Delft, Netherlands
email : y.nishitsuji@tudelft.nl

ABSTRACT

No conclusive evidence has been presented to date for tectonic tremor (TT) in the vicinity of central Chile, where the Nazca Plate is subducting beneath the South American Plate. Subduction in our experimental location (roughly 35.5º S, 70.5º W) is steep and fairly unobstructed compared to the flattened and more seismogenic behavior to the north. We seek to identify TT in our experimental area, whose geodynamics are comparable to tremor-rich subduction zones such as Cascadia and the Nankai Trough. Our method combines time-series visual inspection, frequency-spectrum analysis, waveform cross-correlation, and 3-component (3C) signal covariance to explore the presence of TT in this region. We have identified TT using stations in central Chile and the Malargüe region, Argentina. The TT exhibits similar features to other TT observations worldwide. Waveform characteristics for the TT in our study, particularly dimension of the 3C signal covariance, vary as a function of apparent source location. The duration of one episode of identified TT was about 10 hours, which may indicate that the plate interface where tremor generates is strongly coupled. We conclude that our observations reflect features of the local propagation, rather than the tremor source itself.

Highlights

- Tectonic tremor is identified in central Chile and central western Argentina.
- Principal-component analysis of 3-component signal helps for seismic characterization.
- Identified tremor duration suggests strong coupling of plate interface.

Keywords

Geophysics; tectonic tremor; principal-component analysis; cross-correlation; Argentina

1. INTRODUCTION

Tectonic tremor (TT), which is also known as non-volcanic tremor, is a seismological phenomenon often associated with subduction zone dynamics (e.g. Manea et al., 2013) and it is typically indicative whether there is a transition between seismic and aseismic zones (e.g., Rubinstein et al., 2007; Zigone et al., 2015; Gao and Wang, 2017). As such, its presence may provide insights into cumulative differential strain rates between the tremor-rich portions of a convergent margin and a nearby, geologically different, section that exhibits more stick-slip behavior and associated earthquake behavior (e.g. Brudzinski et al., 2010; Graham et al., 2014). TT was originally discovered by Obara (2002) in the Nankai subduction zone, southwest Japan. Subsequently the phenomenon was identified at numerous other convergent plate margins. Examples include the Cascadia (e.g. Rubinstein et al., 2008), Alaska (e.g. Peterson and Christensen, 2009), Mexico (e.g. Husker et al., 2012), northern Costa Rica (e.g. Walter et al., 2011), Taiwan (Chao et al., 2012), New Zealand (Kim et al., 2011), and the Chile ridge subduction zone where the Nazca, the Antarctic, and the South American plates meet (e.g. Gallego et al., 2013). Ide (2012) reported quantitative comparison of TT that occurred in different settings.

Although the mechanism of TT has not been conclusively identified to date, the influence of fluids on the interface friction of the subducting slab is considered to be key (e.g. Ide et al., 2007; Chao et al., 2011). Occurrence of TT worldwide has been observed to correlate with particular slab characteristics such as slab maturity (e.g. Ide 2012). Depths of TT sources generally range from 20-50 km. In Nankai, Japan, it is about 35-45 km (e.g. Obara 2002), 0-45 km in south central Alaska (Peterson et al., 2009), 15-25 km in Taiwan (Chao et al., 2011), 43 km in Guerrero, Mexico (e.g. Cruz-Atienza et al., 2014), 50 km in New Zealand (Fry et al., 2011), and 30-50 km at the Nazca triple junction, Chile (e.g. Ide, 2012).

In our experimental area, we explore the presence of TT where the Nazca Plate exhibits fairly steeply dipping subduction (dipping of 36° at 35° S) (e.g. Burd et al., 2013) but appears to be clearly segmented with an increase in subduction angle at about 100 km depth; it becomes aseismic at about 200 km depth (e.g. see figure 9 in Anderson et al., 2007). This is in contrast to the convergent plate margin just two degrees (~220 km) farther north, where no such down-dipping bend in the slab is evident, and it lies well south of a flexure in the plate where the subduction angle is considerably flatter, based on earthquake relocations by Anderson et al. (2007). Stress studies in this area suggest that there are large membrane stresses in the lateral direction which have pulled the slab in north-south direction (e.g. Creager et al., 1995) facilitated by a wedge-shaped plume beneath (Burd et al., 2013). About 1000 km south from our study region, Ide (2012) reported identification of TT around the Chile triple junction area using a passband of 2-8 Hz.

In order to ascertain the presence of TT, we use four approaches: visual inspection in the time domain, frequency-spectrum analysis, cross-correlation, and principal-component analyses (PCA). While the benefit of using visual inspection, frequency analysis, and cross-correlation is the straightforward interpretation using them independently or collectively (e.g. Shelly et al., 2007; Kim et al., 2011; Chao et al., 2012), using PCA for interpretation might be not so straightforward. In the sense of hodogram analysis, PCA provides information whether a signal is dominantly (i) linear, (ii) circular, or (iii) spherical in the nature of the detected particle motion. However, characterization of TT in terms of PCA depends on the specific configuration between a TT location and the receivers used to characterize it. Because of that, previous studies found differing features describing the different detected TT using PCA (Maceira et al., 2010; Cruz-Atienza et al., 2015). Therefore, it is difficult to predict beforehand how TT would be described in terms of PCA features. Nevertheless, the observed PCA features will be useful for TT characterization, especially when combining PCA with the other three methods mentioned above.

The Maule, Chile earthquake (27 February 2010, M_W 8.8) occurred about 200 km to the west of Malargüe, Argentina (Fig. 1), on the interface between the subducting Nazca plate and the overriding South American plate. TT has not yet been documented in this area, hence it is of interest to determine whether it occurs here, and if so, how its presence relates to the geodynamic processes influencing nearby seismicity. Ide (2012) speculates that TT (if any) may contribute to our understanding of any relationship between TT and megathrust-type earthquakes. Our primary motivation in this study is to ascertain whether TT is observed near the Maule rupture (e.g. Lorito et al., 2011) and what this may imply for ongoing seismic hazard in this region. By identifying TT in this area we hope to contribute to ongoing investigations to better evaluate the interplate dynamics and possible implications for deformation and corresponding seismic behavior.

2. Study area and data

Fig. 1 shows the location of central Chile and the Malargüe region, Argentina where the Nazca plate is subducting beneath the South American plate towards the southeast. The epicenter of the Maule earthquake (a star in Fig. 1, https://earthquake.usgs.gov/earthquakes/) and the local earthquakes from 1906 until 2014 are also shown. The seismic array we mainly used, MalARRgue (Ruigrok et al., 2012; Nishitsuji et al., 2014), consists of two linear arrays: the TN-array of 19 stations (from TN02 to TN20; light gray triangles in Fig. 1) and the TE-array of 13 stations (from TE01 to TE13; dark gray triangles in Fig. 1), and one irregular array – the PV-array containing 6 stations (from PV01 to PV06; white triangles in Fig. 1). The active volcano Peteroa is situated just west of the PV-array (Casas et al., 2014).

MalARRgue comprised three-component short-period (2 Hz) sensors. These were Sercel L-22 instruments obtained from Incorporated Research Institutes in Seismology (IRIS). Data were recorded on RefTek RT 130 dataloggers at 100 samples per second, and retrieved periodically at irregular visits of the stations during the the deployment. For the purpose of detecting TT, these sensors were deemed adequate because the typical frequencies observed for these signals are of the order of 2-8 Hz (Ide, 2012).

To expand the footprint of our analysis and assess TT more widely, we included in our analysis three more stations located in Chile roughly parallel to the subduction direction of the Nazca plate, as these stations are relatively close to MalARRgue. The three stations (Fig. 1) are GO05 (Nanometrics Trillium 240) from the Chilean National Seismic Network and TEN and AD2 (Guralp 6TD) from the seismic network operated by Observatorio Volcanológico de los Andes del Sur from SERNAGEOMIN (OVDAS-SERNAGEOMIN). We refer to the vertical component of TEN as TENZ in this paper.

3. Principal component analysis

We apply Principal-component analysis to characterize time-varying polarization features of the three-component seismic data. By this process, we can characterize seismic signal variations that are difficult to interpret visually for characteristic patterns in the original traces. This technique is not new to seismology (e.g. Perelberg and Hornbostel, 1994), and in fact has been exploited in studies ranging from instantaneous phase detection (Schimmel and Gallart, 2003; Moriya, 2008) to seismic anisotropy via shear wave splitting (Li et al., 2004). While the cross-correlation is the most-used method for finding (repeatable) TT, signal polarization has been also used (e.g. La Rocca et al., 2005; Wech and Creager, 2007; Maceira et al., 2010; Cruz-Atienza et al., 2014). PCA is a primary tool in assessing seismic polarization (also called particle motion or hodogram analysis) (e.g. Scholz et al. 2017), which is the application we employ here. Our application focuses on characterizing signal covariance at a three-component station.

According to Jurkevics (1988) and Aster et al. (1990), the eigenvalues of the covariance matrix of three-component seismic data can be obtained by performing PCA as

$$\lambda_1 + \lambda_2 + \lambda_3 = 1,\ \lambda_1 \geq \lambda_2 \geq \lambda_3 \geq 0, \quad (1)$$

where λ denotes the eigenvalue. From equation (1), the seismic polarization can be expressed in three different categories (Aster, 1990):

$$\begin{cases} Linearity\ : \lambda_1 = 1, \lambda_2 = \lambda_3 = 0 \\ Circularity: \lambda_1 = \lambda_2 = 1/2\,, \lambda_3 = 0, \\ Sphericity : \lambda_1 = \lambda_2 = \lambda_3 = 1/3 \end{cases} \quad (2)$$

where circularity implies planar particle motion (but not necessarily circular), sphericity indicates particle motion in three dimensions (but not necessarily spherical) (Aster, 1990; Maceira et al., 2010). Figure 2 illustrates schematically the polarization endmembers.

4. Data Processing

4.1 Preprocessing

There are numerous earthquakes in the Malargüe region, Argentina, due to the active convergence between the South American Plate and the subducting Nazca slab (Fig. 1). This activity presents challenges in identifying TT. Using the one-year data of MalARRgue (recorded in 2012), we first search for and exclude time periods containing arrivals from identified local earthquakes whose epicentral distance from our stations is less than 20°, using the event catalogue provided by the IRIS interactive data extraction tool, Java version of Windows Extracted from Event Data (JWEED) which includes the United States Geological Survey (USGS) database. We note here that the catalog is incomplete and our remaining data window will be contaminated by small, near-constant small aftershocks from major interplate earthquakes that have occurred in recent years; hence our TT search is constrained to high-amplitude TT occurrences. This search-and-exclude procedure is repeated for earthquakes whose epicentral distance is larger than 20°. For these events, we remove all events with M > 5.0, assuming that remaining smaller event codas will be insignificant compared to TT amplitude at our stations. Examples of both the local and global (epicentral distance > 120°) events recorded by one PV-array station are shown in Figure S1. We removed `5000 events from the acquisition period in 2012.

We further excluded time intervals when the wind was strong. Previous examination of the MalARRgue data (Nishitsuji et al., 2016b; Weemstra et al., 2017) determined the dominant frequency of the secondary oceanic microseisms to be around 0.3 Hz (Fig. S1), consistent with global norms (Longuet-Higgins, 1950). The microseisms peak for TEN and AD2 is even a bit lower. These peaks are well below the frequency range for TT. Hence, we do not consider microseism in this analysis.

4.2 Visual inspection and frequency analysis

For the waveform cross-correlation, TT templates were chosen via visual inspection in both the time and frequency domains. Since we do not know the direction of wave propagation from TT in this area and also for the sake of data reduction, we used the vertical component for the inspection purpose. Another reason is that when the TT sources are assumed to be located at depths of 30-40 km around the subducting slab, direct S-waves will propagate nearly horizontally due to the distance from the source locations to the arrays meaning that SV waves will be recorded on the vertical component. But the orthogonal components can be used as well. We identified a TT from 15 February 2012 (Fig. 3). This occurrence is observed at five TN stations (TN08, 09, 10, 11, and 12); the other stations of this array were not yet installed. TT is also visible at the TE-array as shown in Figure 4. The TN-array seems to provide higher signal-to-noise ratio than the TE-array due to a combination of stronger, persistent local noise sources at the TE-array, the relatively shorter epicentral distance from TT to the TN stations, and complex site effects at the TE-array arising from variation of the thickness of the sedimentary basin (Nishitsuji et al., 2014; Nishitsuji et al., 2016b)

We determine the optimal passband for filtering our data to be 3-10 Hz by comparing a suite of narrow-band realizations of the waveforms (Fig. 5). This allows us to identify which frequency components of our signal appear to arise from TT, as opposed to other signals or noise (e.g. Fig. 3). For example, one strong peak (the arrow in Fig. 5) was sufficiently suppressed after the filtering. Our choice is similar to, but a few Hz wider than, choices made in some previous studies (e.g. Brown et al., 2009; Tang et al., 2010); our choice though is narrower than choices in other studies: 0.5-10 Hz (Cruz-Atienza et al., 2015), 1-10 Hz (Husker et al., 2012), and 2-10 Hz (Watanabe et al., 2007). Note that exact corners of the passband are difficult to define because they are essentially connected to the specific configurations of TT sources and receiver arrays that examine them. Following the filter selection, data were filtered, demeaned and detrended.

Assuming that the TT we have identified is propagated from the Nazca slab, it should be visible also at the PV array. A comparison of the frequency spectrum of three stations chosen from each of the three MalARRgue arrays is shown in Figure 6. Based on the previous observation regarding the dominant frequency (Fig. 5), background noise at station PV03 in Figure 6 seems to mask the signal of the TT. This noise may represent volcanic tremor generated by the Peteroa Volcano (Casas et al., 2014), or the frequent small aftershocks from the subduction zone ~300 km to the west, whose codas often overlap. Thus, the PV array appears to be less suitable for the identification of TT than the two linear arrays of MalARRgue. Note that high-frequency peaks around 15 Hz and 35 Hz in Figure 6e-f contribute marginally to the appearance of TT because our band-pass filtering between 3-10 Hz keeps the original appearance of TT (Fig. S2).

In Figure 7, we show a comparison of the TT among the five stations selected from all seismic arrays in the central Chile region and the Malargüe region, Argentina. The distance from GO05 (westernmost) to TE11 (easternmost) in Figure 7 is about 250 km. After finding a TT, we perform the waveform cross-correlation and PCA to characterize it further.

4.3 Waveform cross-correlation and PCA

In the geophysics community, waveform cross-correlation is sometimes used to create virtual shot gathers using seismic interferometry (e.g. Claerbout, 1968; Campillo and Paul, 2001; Wapenaar, 2004), often to detect similar signals (patterns) with respect to a given template (e.g. Geller and Mueller, 1980; Obara, 2002; Rowe et al., 2004; Shelly et al., 2006, 2007; Stankova et al., 2008; Wech and Creager, 2008), or to aid in advanced analysis of similar events (Rowe et al., 2002). When using TT template-matching, there are two distinct purposes: identification of long-duration windows (Obara, 2002; Wech and Creager, 2008) and identification of repeating short-duration low-frequency earthquakes (e.g. Shelly et al., 2007). Our goal is template-matching for short duration but we do not look for low-frequency earthquakes. A band-passed master waveform is correlated against band-passed windows of the continuous data. Note that we have removed the instrument response from the recorded data, but this process is not required for the cross-correlation, as waveform segments are normalized. Following Shelly et al. (2007), we set up the master length to be 4 s that is taken where the TT is present across the different stations (rectangular in Fig. 7). We test also correlation with other lengths - from 5 to 8 s, yet they basically affected only the base level. Then we chose the time step of the correlation to be 20 s. Because our aim is to investigate the presence of TT rather than detecting low-frequency events in the TT, we did not fix a threshold of the correlation coefficient, but we might still anticipate a correspondence between correlation coefficient and other time-varying analyses, such as the PCA results.

The same window length and step used in the correlation are applied to compute PCA. Following Maceira et al. (2010), we show the polarization azimuth, linearity, and circularity, which also can be viewed as linearity or planarity, of the PCA (see equation 2). The computed bi-directional azimuth ranges from -90 to 90 degrees. For positive values, 0 and 45 degree mean north-south and northeast-southwest directions, respectively. For negative values, on the contrary, -45 degree means northwest-southeast direction. We present enveloped cross-correlation, PCA and waveform data at the TN-array in Figure 8. In Figure S3, a summary of our processing flow is shown.

5. Discussion

Several studies have applied different methods to detect TT in various settings. Besides the visual inspection of time-series seismograms and their frequency-spectrum analysis, Shelly et al. (2006), for example, applied cross-correlation using time-series templates, whilst Obara (2002) used the envelope cross-correlation. An alternative approach is to use PCA, e.g., Wech and Creager (2007) and Maceira et al. (2010).

We combine the visual inspection, frequency-spectrum analysis, cross-correlation, and PCA methods to identify and characterize TT in the vicinity of the central Chile region and central western Argentina where conclusive evidence of tremor has not been reported yet.

The PCA yields information about particle motion of the TT. For the TN-array in Figure 8, high linearity appears to correspond to the presence of TT. The high linearity in Figure 8 is linked to a narrow range of the polarization azimuth, providing specific direction of the particle motion. For instance, while the azimuth values from TN08 to TN09 concentrate around zero degrees (the solid arrows in the figure), it is around -40 degree at both TN10 and TN12, while TN11 shows it to be about 50-60 degrees. Because the site effect at the TN array is fairly consistent (Nishitsuji et al, 2014; Nishitsuji et al., 2016b), an abrupt change of azimuth is not expected, especially with the 2-km spacing of the TN-array. Hence, local noise might be contaminating the azimuthal change interfering the actual signature of the TT. In order to use PCA to evidence TT, separating the influence of the background before applying PCA should be a prime consideration. Possible contributors to the background in this region are the microseisms, surface waves, body waves from earthquakes, and wind. The microseisms and the surface waves are expected to be below 0.3 Hz (Nishitsuji et al., 2016) and 0.5 Hz (Weemstra et al., 2017), respectively. As introduced earlier in the data processing above, we excluded local, regional, and global earthquake events. For that, we applied a band-pass filter of 3-10 Hz. We also excluded the data which experienced strong wind. The remaining background may contain incoherent random noise due to wild, grazing animals, anthropogenic noise, etc. We therefore rely upon detecting a change to PCA characteristics, rather than any particular characteristic of the intrinsic PCA, to target likely instances of TT compared to general background signatures, and we compare the changes observed with more than one observable to make our determination.

TN08 and TN11 exhibit a higher cross-correlation coefficient where TT is visible in Figure 8 (the dotted arrows in the figure); however, correlation appears to be generally less informative than the other methods. This could be due to the time step of the correlation we used and/or the data length. For the time step, we conducted a test by changing the time step to be 10 s, 2 s, and 0.5 s (Figure S4). But the results only boosted the base level, which essentially has no effect (Watanabe et al., 2007). As for the data length, while past studies (e.g. Shelly et al., 2007) displayed 20-s- to 1-hour-long data, we scan and display 24 hours of data taken from the one-year-long MalARRgue acquisition. Therefore, in Figure S5 we show a 30-minute window around the master trace where the correlation coefficient equals one (rectangle in Fig. 8). For Figure S5, we used a 4 s window length (the identical master used in Fig. 8) and 2 s steps for both the correlation and PCA. It emerged that several pulse-like signals of seismic amplitude within the identified TT seem to correspond with higher coefficients (the gray rectangles in Fig. S5) but not significantly. Therefore, the results of the cross-correlation are not used as an evidence of TT.

Looking at other PCA results from the TE-array as shown in Figure 9, circularity appears to be generally dominant compared to linearity. Since TE11 shows the highest cross-correlation coefficient with good correspondence of bimodal azimuth towards ± 90 degree, we use this station in the comparison in Figure 10. One of major reasons that TE11 shows such high correlation coefficient could be explained by little interference from local noise. However, we do not mean that the quality of other stations of the TE-array is necessarily inferior.

In Figure 10, we show a comparison of the analysis result for stations across central Chile and Argentina in a way similar to that in Figure 8. The comparison shows that high linearity seems to be corresponding to the emergence of TT. However, for GO05, where the Nazca slab starts to subduct (e.g. Pesicek et al., 2012; Dannowski et al., 2013), circularity is dominant compared to linearity (similar to TE11).

There is no conclusive explanation how TT should be characterized by PCA. While Maceira et al. (2010) found that TT corresponded to low linearity, Cruz-Atienza et al. (2015) found it to correspond to high linearity. We observe both cases, i.e., GO05 shows low linearity (high circularity) while TN11 exhibits high linearity (low circularity). In order to interpret the current PCA results, information about the source location of the TT would be helpful, as the specific characteristic of higher linearity or higher circularity may be a function of the position of a station relative to the source. Our receiver configuration is inadequate to locate TT due the limited spatial distribution. Specifically, TN- and TE-arrays consist of 19 stations spaced at 2 km and 13 stations spaced at 4 km, respectively. As various researchers, including Ryberg et al. (2010) and Chao et al. (2013), have stated, hypocentral determination of TT (especially in depth) is a laborious task using conventional methods, due to the lack of clear body-wave arrivals (e.g. Ito et al., 2007; Shelly et al., 2007). Therefore, as argued in Peterson and Christensen (2009), uncertainties in estimating the source locations can be large. Despite such difficulties, we estimate TT locations using CrazyTremor (Chao and Yu, 2018), and show the results in Figures 10 and S6. CrazyTremor locates TT based on a method which minimizes the root-mean-square value between a theoretical travel time, which is adapted from the CORAL tool for seismology (Wech and Creager, 2008), and a picked travel time. A number of studies used this approach and succeeded in identifying TT (e.g., Peng and Chao, 2008; Peng et al., 2009; Chao et al., 2012; Tang et al., 2017; Chao and Yu, 2018). In addition to its proven performance, we used CrazyTremor because it is computationally efficient when handling large datasets. More details including its graphical user interface can be found in Chao and Yu (2018) and references therein. From these figures and what we discuss above, the Nazca plate subduction zone is the best candidate for the TT identified in this study.

The depth of the slab beneath GO05 is expected to be 40-70 km, whereas it is 100-150 km beneath the PV-array (Nishitsuji et al., 2016a). Since the range of hypocentral depths of other TT at different slabs are varying at 20-50 km (e.g. Ide, 2012), the higher circularity at GO05 can be explained by the short distance from the TT location. This means that the polarization becomes a scatter assuming the source is situated beneath GO05 or in its neighborhood. On the contrary, the higher linearity at PV03, TENZ, and TN11 can be related to the longer distance. In other words, the scattering strength becomes weak as a function of distance between the source and receiver. Such linearity no longer persists, however, at TE11 and most of the TE-array. This could be because the signals themselves become weaker towards the east so that it is difficult to observe the high linearity due to interference from local noise. Note that the amplitude range at the TN- and TE-arrays in Figures 8 and 9 is identical.

The duration of the TT is observed to vary among regions and individual TT observations around the world (e.g. Peterson and Christensen, 2007). For instance, Gallego et al. (2013) reported that the duration ranges from less than 10 hours to up to 48 hours for the Chile triple junction region, whilst Husker et al. (2012) found it to be from less than a minute to days for Mexico. In our case, although we identified only one episode, the duration is around 10 hours (the TT episode is indicated by the magenta rectangle in Fig. 10). Our TT episode might comprise a series of discrete, overlapping, low frequency events, but this study does not investigate that possibility.

TT duration is hypothesized to correspond to the width of the TT zone in the subducting direction (e.g. Ide et al., 2012), the shear stress (fluid flow) status (e.g. Shelly et al., 2006; Brown et al., 2009), and the tidal stress (e.g. Ide et al., 2012; Gallego et al., 2013), but not necessarily (Ide, 2010). According to Ide (2010), a shorter duration of TT possibly indicates that a tremor zone could be characterized by a brittle rupture, whereas a longer duration could be related to a so-called diffusive slip (migration). These two distinct features maybe associated with the Moho where the serpentinization is considered to begin (e.g. Ide, 2010). Following this interpretation line, the TT duration we observed could be seen as a gauge for helping understand such geodynamics in this particular region where the Maule earthquake has occurred. The TT duration we found is not short, like of the order of seconds or minutes, but lasts for 10 hours. Thus, this might be interpreted to indicate that the tremor zone we capture is characterized by a rather ductile behavior. Nonetheless, since the ductile interpretation is mainly driven by conceptual models, an alternative, yet possibly more plausible, interpretation is the magnitude of the aseismic slip (Aguiar et al., 2009; Wech et al., 2010; Frank, 2016; Thomas et al., 2018). Furthermore, the cross-correlation results in Figure 8 indicate apparent lack of repeating events (low-frequency earthquakes) that would correlate during the TT and render waveform correlation to be useful in detecting TT. This lack of repeating events might also be connected to the size of the TT zone. Studies which found repeatable events during TT (e.g. Shelly et al., 2007; Maceira et al., 2010) suggest that common source mechanism is excited at common or nearby asperities. A lack of repeating events suggests varying source mechanisms or distributed source locations i.e., they are not controlled by stress concentration at asperities that repeatedly slip. Although the interpreted TT duration and a lack of repeating events inferred by failure of cross-correlation does not exclude common physics, more TT samples and their spatial-time localizations are certainly required to perform a more plausible and quantitative interpretation.

Our TT detections in this region (e.g. Fig. 7) share similar features to those described in other TT studies (e.g. La Rocca et al., 2005; Tang et al., 2010): (1)

dominant frequency concentrated from a few Hz to 10 Hz; (2) long event duration; (3) subtle amplitude but higher than that of the ambient noise; (4) incoherent phase. These commonalities are consistent with our interpretation of the phenomenon we see as TT. Integrating different methods (time-series inspection, frequency-spectrum analysis, waveform cross-correlation, and PCA) helped us identify and characterize TT. For more rigorous investigation, however, including the source mechanism and location, appropriate receiver arrays in the central Chile and Malargüe, Argentina, are essential to elucidate the possible relationship between TT and megathrust-type earthquakes for the Nazca slab.

6. Conclusions

We used visual inspection of time series, frequency-spectrum analysis, waveform cross-correlation and principal component analysis (PCA) to identify and characterize tectonic tremor (TT) in the central Chile and Malargüe region of central western Argentina, where conclusive evidence of subduction-related TT has not been previously observed. Our results show similar features to other TT occurrences worldwide, supporting the hypothesis that TT is occurring in our study area. The duration of the TT episode we observed is about 10 hours, which might be indicative of a rather ductile behavior of the TT zone.

Acknowledgements

The authors thank two anonymous reviewers for their constructive comments that improved the quality of this manuscript. The authors are also thankful to Kevin Chao for his help with using CrazyTremor. Seismic Analysis Code (SAC) was used for a part of data processing. The maps were drawn with GenericMappingTool (GMT) (Wessel and Smith, 1991) and MATLAB. This is Los Alamos National Laboratory Publication LA-UR-19-20128.

References

Aguiar, A.C., Melbourne, T.I., and Scrivner, W., 2009. Moment release rate of Cascadia tremor constrained by GPS. Journal of Geophysical Research, 114, B00A05, doi:10.1029/2008JB005909.

Anderson, M., Alvarado, P., Zandt, G., and Beck, S., 2007. Geometry and brittle deformation of the subducting Nazca Plate, Central Chile and Argentina. Geophysical Journal International, 171, 419–434, doi: 10.1111/j.1365-246X.2007.03483.x.

Aster, R.C., Shearer, P.M., and Berger, J., 1990. Quantitative measurements of shear wave polarizations at the Anza Seismic Network, southern California: implications for shear wave splitting and earthquake prediction. Journal of Geophysical Research, 95, 12449-12473, doi:10.1029/JB095iB08p12449.

Brown, J.R., Beroza, G.C., Ide, S., Ohta, K., Shelly, D.R., Schwartz, S.Y., Rabbel, W., Thorwart, M., and Kao, H., 2009. Deep low-frequency earthquakes in tremor localize to the plate interface in multiple subduction zones. Geophysical Research Letters, 36, L19306, doi:10.1029/2009GL040027.

Brudzinski, M.R., Hinojosa-Prieto, H.R., Schlanser, K.M., Cabral-Cano, E., Arciniega-Ceballos, A., Diaz-Molina, O., and DeMets, C., 2010. Nonvolcanic tremor along the Oaxaca segment of the Middle America subduction zone. Journal of Geophysical Research, 115, B00A23, doi:10.1029/2008JB006061.

Burd, A.I., Booker, J.R., Mackie, R., Pomposiello, C., and Favetto, A., 2013. Electrical conductivity of the Pampean shallow subduction region of Argentina near 33 S: evidence for a slab window. Geochemistry, Geophysics, Geosystems, 14, 3192-3209, doi: 10.1002/ggge.20213.

Campillo, M., and Paul, A., 2003, Long-range correlations in the diffuse seismic coda. Science, 299, 547–549, doi: 10.1126/science.1078551.

Casas, J.A., Badi, G., Manassero, M.C., Gòmez, M., Draganov, D., and Ruzzante, J., 2014. Characterization of seismo-volcanic activity in Peteroa Volcano, Central Andes Argentina-Chile. Earth Sciences Research Journal, 18, Special Issue (July, 2014), 335-336. ISBN: 1794-6190.

Chao, K., Peng, Z., Wu, C., Tang, C.-C., and Lin, C.-H., 2011. Remote triggering of non-volcanic tremor around Taiwan. Geophysical Journal International, 188, 301-324, doi:10.1111/j.1365-246X.2011.05261.x.

Chao, K., Peng, Z., Fabian, A., and Ojha, L., 2012. Comparisons of triggered tremor in California, Bulletin of the Seismological Society of America, 102, 900-908, doi:10.1785/0120110151.

Chao, K., Peng, Z., Gonzales-Huizar, H., Aiken, C., Enescu, B., Kao, H., Velasco, A.A., Obara, K., and Matsuzawa, T., 2013. A global search of triggered tremor following the 2011 Mw9.0 Tohoku-Oki earthquake. Bulletin of the Seismological Society of America, 103, 1551-1571, doi:10.1785/0120120171.

Chao, K., and Yu, C., 2018. A MATLAB GUI for examining triggered tremor: A case study in New Zealand. Seismological Research Letters, 89, 2362-2373, doi: 10.1785/0220180057.

Claerbout, J., 1968. Synthesis of a layered medium from its acoustic transmission response. Geophysics, 33, 264-269, doi:10.1190/1.1439927.

Creager, K.C., Chiao, L., Winchester, J.P., and Engdahl, E.R., 1995. Membrance strain rates in the subducting plate beneath South America. Geophysical Research Letters, 22, 2321-2324, doi:10.1029/95GL02321.

Cruz-Atienza, V.M., Husker, A., Legrand, D., Caballero, E., and Kostoglodov, V., 2015. Nonvolcanic tremor locations and mechanisms in Guerrero, Mexico, from energy-based and particle motion polarization analysis. Journal of Geophysical Research, 120, 275-289, doi:10.1002/2014JB011389.

Dannowski, A., Grevemeyer, I., Kraft, H., Arroyo, I., and Thorwart, M., 2013. Crustal thickness and mantle wedge structure from receiver functions in the Chilean Maule region at 35°S. Tectonophysics, 592, 159-164, doi:10.1016/j.tecto.2013.02.015.

Frank, W.B., 2016. Slow slip hidden in the noise: The intermittence of tectonic release. Geophysical Research Letters, 43, 10125-10133, doi:10.1002/2016GL069537.

Fry, B., Chao, K., Bannister, S., Peng, Z., and Wallace, L., 2011. Deep tremor in New Zealand triggered by the 2010 Mw8.8 Chile earthquake. Geophysical Research Letters, 38, L15306, doi:10.1029/2011GL048319.

Gallego, A., Russo, R.M., Comte, D., Mocanu, V., Murdie, R.E., and VanDecar, J.C., 2013. Tidal modulation of continuous nonvolcanic seismic tremor in the Chile triple junction region. Geochemistry, Geophysics, Geosystems, 14, 14851-14863, doi:10.1002/ggge.20091.

Gao, X., and Wang, K., 2017. Rheological separation of the megathrust seismogenic zone and episodic tremor and slip. Nature, 543, 416-419, doi: 10.1038/nature21389.

Geller, R.J., and Mueller, C.S., 1980. Four similar earthquakes in central California. Geophysical Research Letters, 7, 821-824, doi:10.1029/GL007i010p00821.

Graham, S.E., DeMets, C., Cabral-Cano, E., Kostoglodov, V., Walpersdorf, A., Cotte, N., Brudzinski, M., McCaffrey, R., and Salazar-Tlaczani, L., 2014. GPS constraints on the M_w = 7.5 Ometepec earthquake sequence, southern Mexico: coseismic and post-seismic deformation. Geophysical Journal International, 199, 200-218, doi:10.1093/gji/ggu167.

Husker, A.L., Kostoglodov, V., Cruz-Atienza, V.M., and Legrand, D., 2012. Temporal variations of non-volcanic tremor (NVT) locations in the Mexican subduction zone: finding the NVT sweet spot. Geochemistry, Geophysics, Geosystems, 13, Q03011, doi:10.1029/2011GC003916.

Ide, S., Shelly, D.R., and Beroza, G.C., 2007. Mechanism of deep low frequency earthquakes: further evidence that deep non-volcanic tremor is generated by shear slip on the plate interface. Geophysical Research Letters, 34, L03308, doi:10.1029/2006GL028890.

Ide, S., 2010. Striations, durations, migration and tidal response in deep tremor. Nature, 466, 356-359, doi: 10.1038/nature09251.

Ide, S., 2012. Variety and spatial heterogeneity of tectonic tremor worldwide. Journal of Geophysical Research, 117, B03302, doi:10.1029/2011JB008840.

Ito, Y., Obara, K., Shiomi, S., Sekine, S., and Hirose, H., 2007. Slow earthquakes coincident with episodic tremors and slow slip events. Science, 315, 503-506, doi:10.1126/science.1134454.

Jurkevics, A., 1988. Polarization analysis of three-component array data. Bulletin of the Seismological Society of America, 78, 1725-1743.

Kim, M.J., Schwartz, S.Y., and Bannister, S., 2011. Non-volcanic tremor associated with the March 2010 Gisborne slow slip event at the Hikurangi subduction margin, New Zealand. Geophysical Research Letters, 38, L14301, doi:10.1029/2011GL048400.

La Rocca, M., McCausland, W., Galluzzo, D., Malone, S., Saccorotti, G., and Del Pezzo, E., 2005. Array measurements of deep tremor signals in the Cascadia subduction zone. Geophysical Research Letters, 32, L21319, doi:10.1029/2005GL023974.

Li, X, Sze, E., Burns, D., and Toksoz, N., 2004. S-wave splitting analysis: covariance matrix method and preliminary application. SEG Technical Program Expanded Abstarcts 2004, 151-154, doi: 10.1190/1.1851130.

Longuet-Higgins, M.S., 1950. A theory of the origin of microseisms. Philosophical

Transactions of the Royal Society of London, 243, 1-35.

Lorito, S., Romano, F., Atzori, S., Tong, X., Avallone, A., McCloskey, J., Cocco, M., Boschi, E., and Piatanesi, A., 2011. Limited overlap between the seismic gap and coseismic slip of the great 2010 Chile earthquake. Nature Geoscience, 4, 173-177, doi: 10.1038/NGEO1073.

Maceira, M., Rowe, C.A., Beroza, G., and Anderson, D., 2010. Identification of low-frequency earthquakes in non-volcanic tremor using the subspace detector method. Geophysical Research Letters, 37, L06303, doi:10.1029/2009GL041876.

Manea, V.C., Manea, M., and Ferrari, L., 2013. A geodynamical perspective on the subduction of Cocos and Rivera plates beneath Mexico and Central America. Tectonophysics, 609, 56-81, doi: 10.1016/j.tecto.2012.12.039.

Moriya, H., 2008. Precise arrival time detection of polarized seismic waves using the spectral matrix. Geophysical Prospecting, 56, 667-676, doi: 10.1111/j.1365-2478.2008.00713.x.

Nishitsuji, Y., Ruigrok, E., Gòmez, M., and Draganov, D., 2014. Global-phase H/V spectral ratio for imaging the basin in the Malargüe region, Argentina. Seismological Research Letters, 85, 1004-1011, doi: 10.1785/0220140054.

Nishitsuji, Y., Ruigrok, E., Gòmez, M. Wapenaar, K., and Draganov, D., 2016a. Reflection imaging of aseismic zones of the Nazca slab by global-phase seismic interferometry. Interpretation, 4, SJ1-SJ16, doi:10.1190/int-2015-0225.1.

Nishitsuji, Y., Minato, S., Boullenger, B., Gòmez, M., Wapenaar, K., and Draganov, D., 2016b. Crustal-scale reflection imaging and interpretation by passive seismic interferometry using local earthquakes. Interpretation, 4, SJ29-SJ53, doi:10.1190/int-2015-0226.1.

Obara, K., 2002. Nonvolcanic deep tremor associated with subduction in southwest Japan. Science, 296, 1679-1681, doi:10.1126/science.1070378.

Peng, Z., and Chao, K., 2008. Non-volcanic tremor beneath the Central Range in Taiwan triggered by the 2011 M_{W} 7.8 Kunlun earthquake. Geophysical Journal International, 175, 825-829, doi:10.1111/j.1365-246X.2008.03886.x.

Peng, Z., Vidale, J.E., Wech, A.G., Nadeau, R.M., and Creager, K.C., 2009. Remote triggering of tremor along the San Andreas faults in central California, Journal of Geophysical Research, 114, B00A06, doi:10.1029/2008JB006049.

Perelberg, A.I., and Hornbostel, S.C., 1994. Applications of seismic polarization analysis. Geophysics, 59, 119-130, doi: 10.1190/1.1443522.

Pesicek, J.D., Engdahl, E.R., Thurber, C.H., DeShon, H.R., and Lange, D., 2012. Mantle subducting slab structure in the region of the 2010 M8.8 Maule earthquake (30-40°S) Chile. Geophysical Journal International, 191, 317-324, doi:10.1111/j.1365-246X.2012.05624.x.

Peterson, C.L., and Christensen, D.H., 2009. Possible relationship between nonvolcanic tremor and the 1998-2001 slow slip event, south central Alaska. Journal of Geophysical Research, 114, B06302, doi:10.1029/2008JB006096.

Rowe, C.A., Aster, R.C., Phillips, W.S., Jones, R.H., Borchers, B., and Fehler, M.C., 2002. Using automated, high-precision repicking to improve delineation of microseismic structures at the Soultz geothermal reservoir. Pure Applied Geophysics, 159, 563-596, doi: 10.1007/PL00001265.

Rowe, C.A., Thurber, C. H., and White, R. A., 2004. Dome growth behavior at Soufriere Hills Volcano, Montserrat, revealed by relocation of volcanic event swarms, 1995-1996, Journal of Volcanology and Geothermal Research, 134, 199-221, doi:10.1016/j.jvolgeores.2004.01.008.

Rubinstein, J.L., La Rocca, M., Vidale, J.E., Creager, K.C., and Wech A.G., 2008. Tidal modulation of nonvolcanic tremor. Science, 319, 186-189, doi:10.1126/science.1150558.

Rubinstein, J.L., Vidale, J.E., Gomberg, J., Bodin, P., Creager, K.C., and Malone, S.D., 2007. Non-volcanic tremor driven by large transient shear stresses. Nature, 448, 579-582, doi: 10.1038/nature06017.

Ruigrok, E., Draganov, D., Gomez, M., Ruzzante, J., Torres, D., Lopes Pumarega, I., Barbero, N., Ramires, A., Castano Ganan, A.R., van Wijk, K., and Wapenaar, K., 2012. Malargüe seismic array: design and deployment for the temporary array. The European Physical Journal Plus, 127, 126, doi:10.1140/epjp/i2012012126-7.

Ryberg, T., Haberland, C., Fuis, G.S., Ellsworth, W.L., and Shelly, D.R., 2010. Locating non-volcanic tremor along the San Andreas Fault using a multiple array source imaging technique. Geophysical Journal International, 183, 1485-1500, doi:10.1111/j.1365-246X.2010.04805.x.

Schimmel, M., and Gallart, J., 2003. The use of instantaneous polarization attributes for seismic signal detection and image enhancement. Geophysical Journal International, 155, 653-668, doi: 10.1046/j.1365-246X.2003.02077.x.

Scholz, J-.R., Barruol, G., Fontaine, F.R., Sigloch, K., Crawford, W.C., and Deen, M., 2017. Orienting ocean-bottom seismometers from *P*-wave and Rayleigh wave polarizations. Geophysical Journal International, 208, 1277-1289, doi: 10.1093/gji/ggw426.

Shelly, D.R., Beroza, G.C., Ide, S., and Nakamula, S., 2006. Low-frequency earthquakes in Shikoku, Japan, and their relationship to episodic tremor and slip. Nature, 442, 188-191, doi:10.1038/nature04931.

Shelly, D.R., Beroza, G.C., and Ide, S., 2007. Non-volcanic tremor and low-frequency earthquakes swarms. Nature, 446, 305-307, doi:10.1038/nature05666.

Stankova, J., Bilek, S., Rowe, C., and Aster, R., 2008. Characteristics of the October 2005 microearthquake swarm and reactivation of seismic swarms over decade-scale time periods near Socorro, New Mexico. Bulletin of the Seismological Society of America, 98, 93-105, doi:10.1785/0120070108.

Tang, C-.C., Peng, Z. Chao, K. Chen, C-.H., and Lin, C-.H., 2010. Detecting low-frequency earthquakes within non-volcanic tremor in southern Taiwan triggered by the 2005 Mw8.6 Nias earthquake. Geophysical Research Letters, 37, L16307, doi:10.1029/2010GL043918.

Tang, V., Chao, K., and van der Lee, S., 2017. Towards a systematic search for triggered seismic events in the USA. AGU Annual Meeting, New Orleans, Los Angeles, 11-15, p. S23B-0802.

Thomas, A.M., Beeler, N.M., Burgmann, R., and Shelly, D.R., 2018. Using low-frequency earthquake families on the San Andreas Fault as deep creepmeters. Journal of Geophysical Research: Solid Earth, 123, 457-475, doi:10.1002/2017JB014404.

Walter, J.I., Schwartz, S.Y., Protti, J.M., and Gonzalez, V., 2011. Persistent tremor within the northern Costa Rica seismogenic zone. Geophysical Research Letters, 38, L01307, doi:10.1029/2010GL045586.

Wapenaar, K., 2004. Retrieving the elastrodynamic Green’s function of an arbitrary inhomogeneous medium by cross correlation. Physical Review Letters, 93, 254301, doi:10.1103/PhysRevLett.93.254301.

Watanabe, T., Hiramatsu, Y., and Obara, K., 2007. Scaling relationship between the duration and the amplitude of non-volcanic deep low-frequency tremors. Geophysical Research Letters, 34, L07305, doi:10.1029/2007GL029391.

Wech, A.G., and Creager, K.C., 2007. Cascadia tremor polarization evidence for plate interface slip. Geophysical Research Letters, 34, L22306, doi:10.1029/2007GL031167.

Wech, A.G., and Creager, K.C., 2008. Automated detection and location of Cascadia tremor. Geophysical Research Letters, 35, L20302, doi:10.1029/2008GL035458.

Wech, A.G., Creager, K.C., Houston, H., and Vidale, J.E., 2010. Geophysical Research Letters, 37, L22310, doi:10.1029/2010GL044881.

Weemstra, C., Draganov, D., Ruigrok, E.N., Hunziker, J., Gomez, M., and Wapenaar, K., 2017. Application of seismic interferometry by multidimensional deconvolution to ambient seismic noise recorded in Malargüe, Argentina. Geophysical Journal International, 208, 693-714, doi:10.1093/gji/ggw425.

Wessel, P., and Smith, W.H.F., 1991. Free software helps map and display data. Eos, Transactions American Geophysical Union, 72, 441-448, doi:10.1029/90EO00319.

Zigone, D., Ben-Zion, Y., and Campillo, M., 2015. Modelling non-volcanic tremor, slow slip events and large earthquakes in the Guerrero Subduction zone (Mexico) with space-variable frictional weakening and creep. Geophysical Journal International, 202, 653-669, doi:10.1093/gji/ggv174.

Figure captions

Figure 1. : Top: location of the seismic stations used in our study. The black dots denote hypocenters of earthquakes. The red star is the hypocenter of the Maule earthquake (27 February 2010, M_{W} 8.8). Below: distribution of the local earthquakes in depth.

Figure 2. : The classification of seismic polarization. The eigenvalue of λ is calculated by principal component analysis (PCA) in this study.

Figure 3. : The visual inspection of the TT at the TN-array recorded on 15 February 2012. The rectangular denotes the window shown in Figure 5. The other stations of the TN-array (e.g. TN07 and TN13) were not available due to the technical problem of the acquisition.

Figure 4. : Same as Figure 3, but for the TE-array.

Figure 5. : Example of the band-pass filtering (3-10 Hz) for TN11 at 12:46:40 on 15 February 2012 when the TT is present. The arrow indicates an event that is

removed by the filtering. Time window of the dashed rectangle is identical to the interval marked by the magenta rectangles in Figure 6.

Figure 6. : Examples of the time-series on and spectrogram from 15 February 2012 recorded at PV03 station (one of the stations of the PV-array), TN11, and TE08. Magenta rectangles across the power spectral densities of (a), (b), and (c) correspond to the frequency spectrum (TT) of (d), (e), and (f), respectively. The gray rectangle corresponds to the time window shown in Figure S2.

Figure 7. : Time-series comparisons of the TT on 15 February 2012 recorded at five stations shown in Figure 1. The gray rectangle shows the location of the master trace to be cross-correlated.

Figure 8. : Results of PCA and enveloped correlation for the TN-array on 15 February 2012. The gray rectangle shows the sampling area where the master traces are (the coefficients are 1.0). The solid arrows indicate where the azimuth values concentrate around zero degrees. The dotted arrows indicate where a higher cross-correlation coefficient presents.

Figure 9. : Same as Figure 8, but for the TE-array.

Figure 10. : Same as Figure 8, but for the five stations used in Figure 7. A circle in yellow is the estimated TT location for T1 shown in Figure S6. Bars around the circle indicate error ranges. The magenta rectangle indicates the identified TT episode which continues about 10 hours. The red rectangle corresponds to the time window shown in Figure S6.

Figure S1. : Examples of the time-series and spectrograms of local (epicentral distance is less than 20°) and global (epicentral distance is greater than 120°) events recorded at PV03 station (one of the stations of the PV-array). Magenta bars in the power spectral density in (a) and (b) indicate the time intervals used for the frequency analysis in (c) and (d), respectively.

Figure S2. : Comparison of band-pass filtering by (a) 0.1-40 Hz and (b) 3-10 Hz for TE-array.

Figure S3. : Summarized processing flow used in this study.

Figure S4. : Results of enveloped correlation for the TN-array when time steps of 20 s, 10 s, 2 s, and 0.5 s are used of data from 15 February 2012.

Figure S5. : Same as Figure 8, but windowed 30 minutes around the master traces used in Figure 8.

Figure S6. : Picking examples (label T1) based on envelope for TT locations shown in Figure 10.

Fig.1

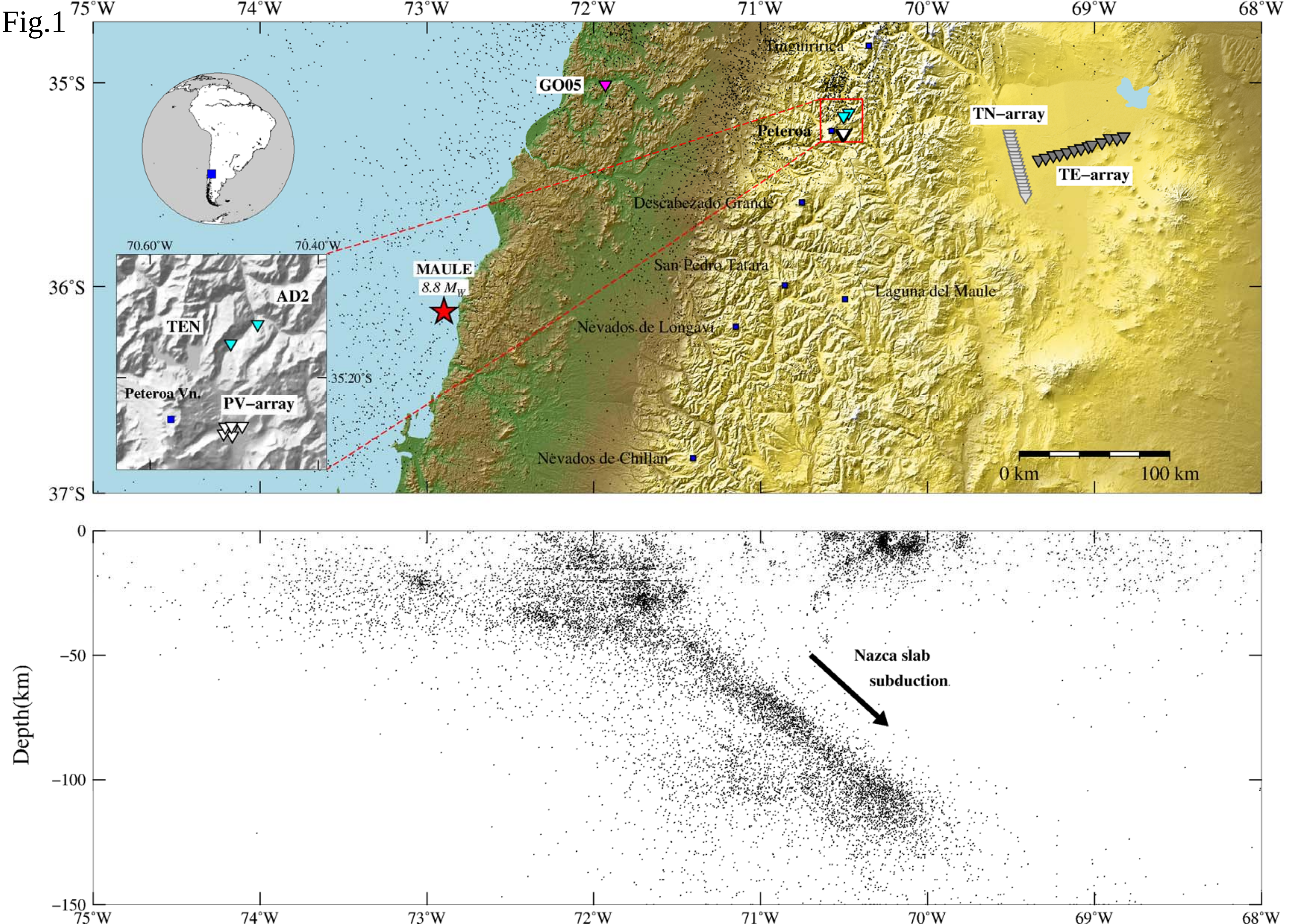

75°W
74°W
73°W
72°W
71°W
70°W
69°W
68°W
35°S
36°S
37°S
GO05
Tinguiririca
Peteroa
TN−array
TE−array
Descabezado Grande
San Pedro Tatara
Laguna del Maule
Nevados de Longaví
Nevados de Chillan
MAULE
8.8 M_W
0 km
100 km
70.60°W
70.40°W
35.20°S
AD2
TEN
Peteroa Vn.
PV−array
Depth(km)
0
−50
−100
−150
Nazca slab
subduction

Fig.2

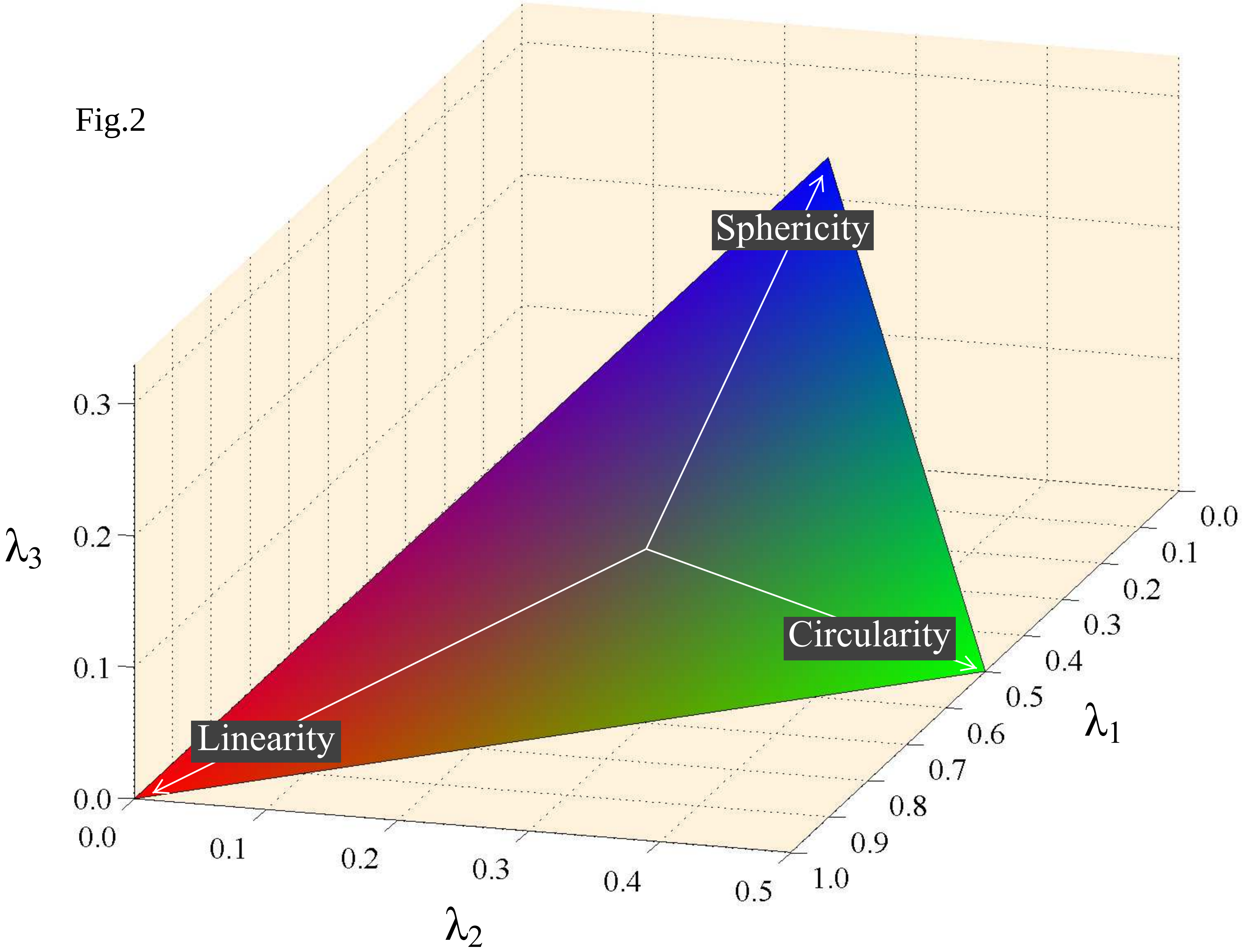

Sphericity
Circularity
Linearity
λ3
0.3
0.2
0.1
0.0
0.0
0.1
0.2
0.3
0.4
0.5
λ2
0.0
0.1
0.2
0.3
0.4
0.5
0.6
0.7
0.8
0.9
1.0
λ1

Fig.3

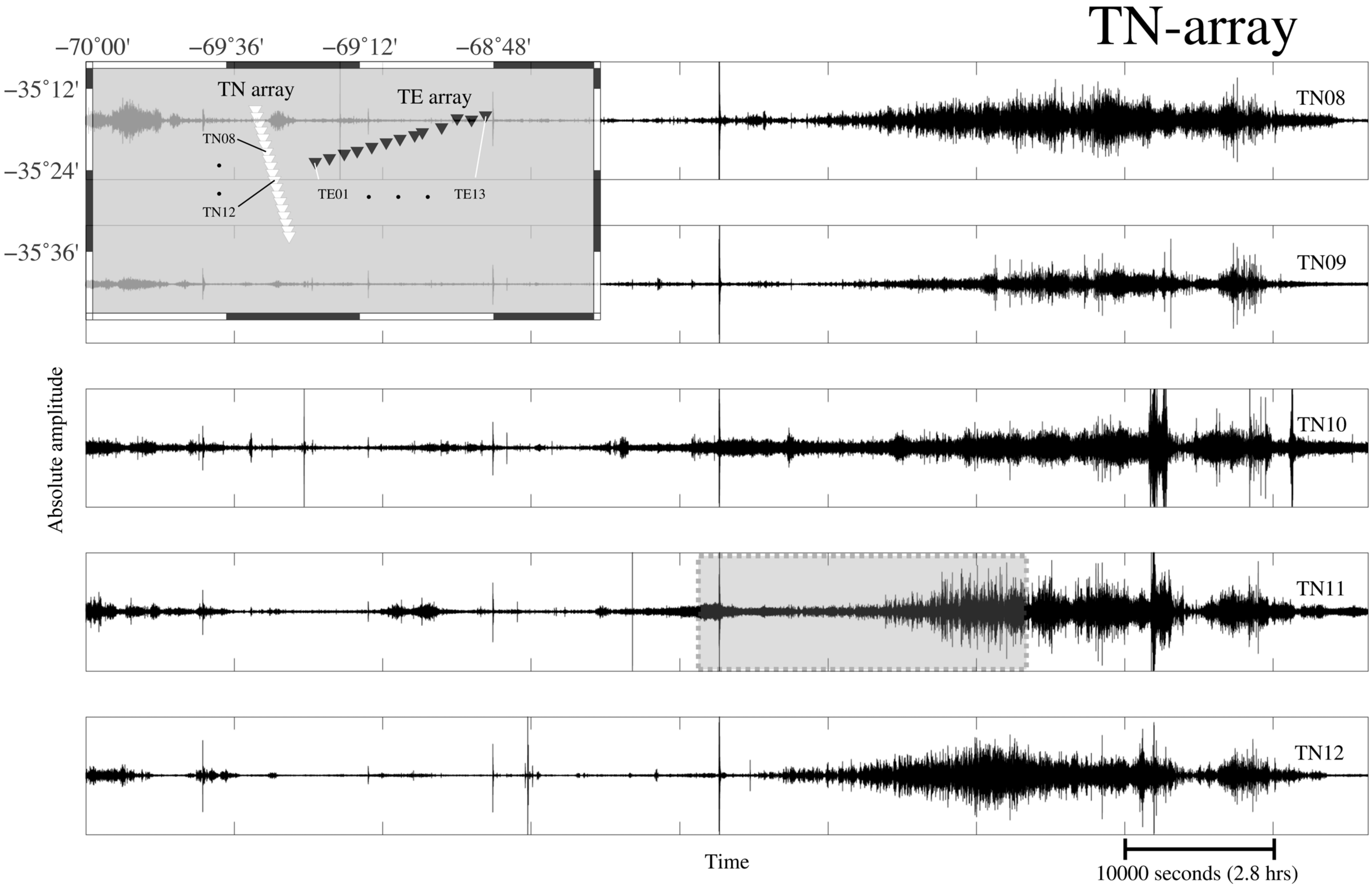
TN-array
−70°00'
−69°36'
−69°12'
−68°48'
−35°12'
−35°24'
−35°36'
TN array
TE array
TN08
TN12
TE01
TE13
TN08
TN09
TN10
TN11
TN12
Absolute amplitude
Time
10000 seconds (2.8 hrs)

Fig.4

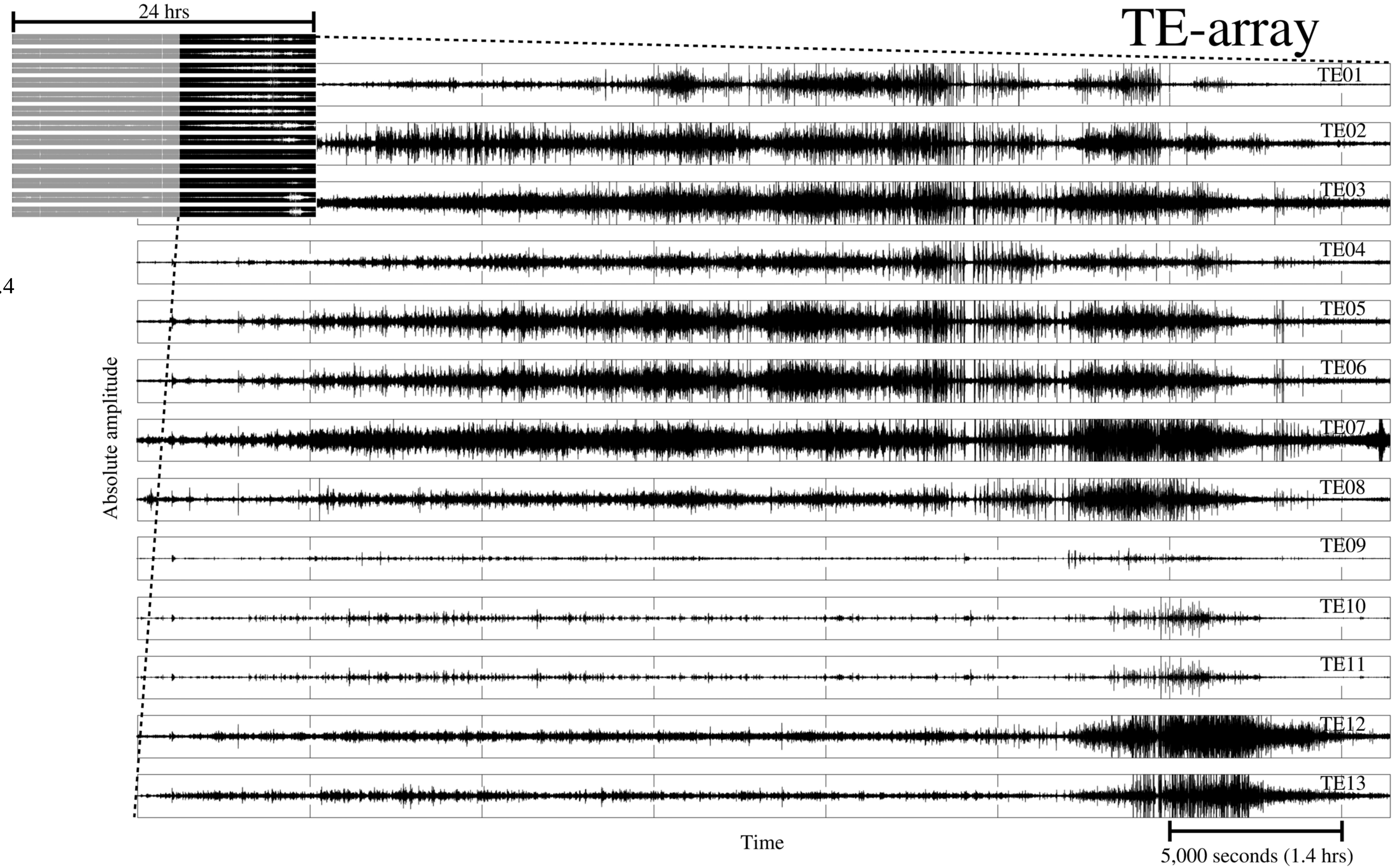
24 hrs
TE-array
TE01
TE02
TE03
TE04
TE05
TE06
TE07
TE08
TE09
TE10
TE11
TE12
TE13
Absolute amplitude
Time
5,000 seconds (1.4 hrs)

Fig.5

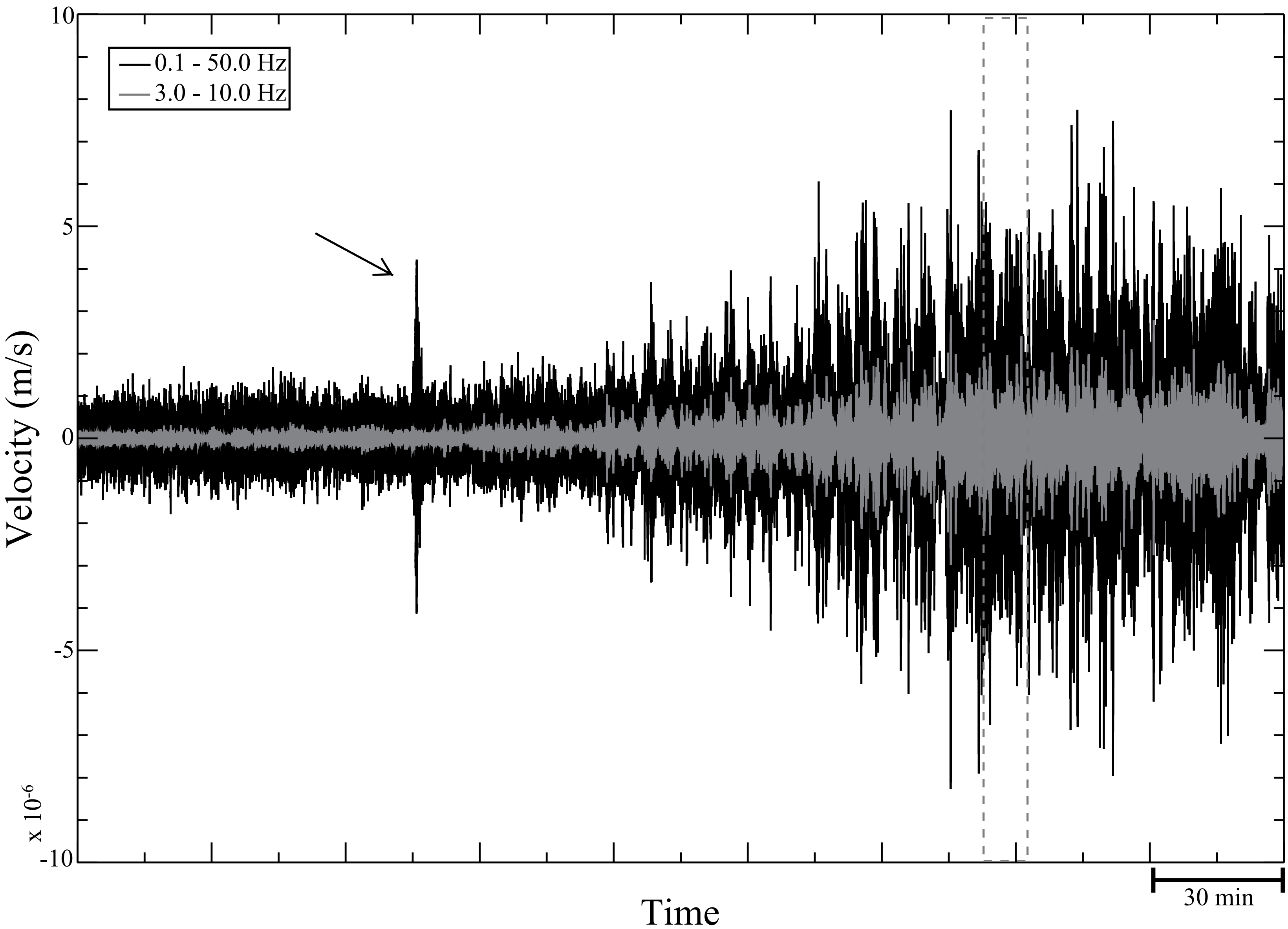

Fig.6

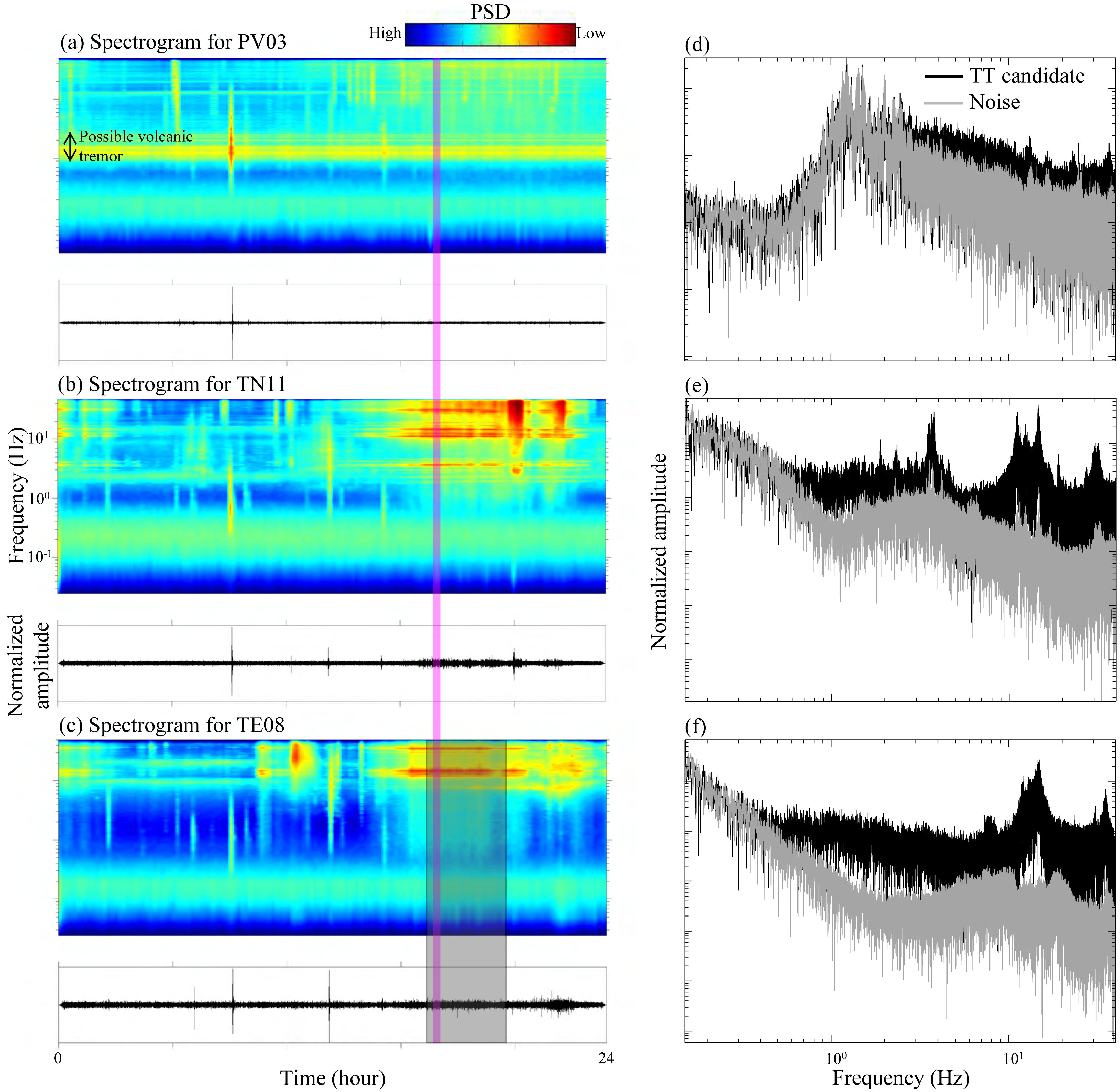
PSD
High
Low
(a) Spectrogram for PV03
Possible volcanic
tremor
(b) Spectrogram for TN11
(c) Spectrogram for TE08
Frequency (Hz)
10^1
10^0
10^{-1}
Normalized
amplitude
0
24
Time (hour)
(d)
TT candidate
Noise
(e)
(f)
Normalized amplitude
10^0
10^1
Frequency (Hz)

Fig.7

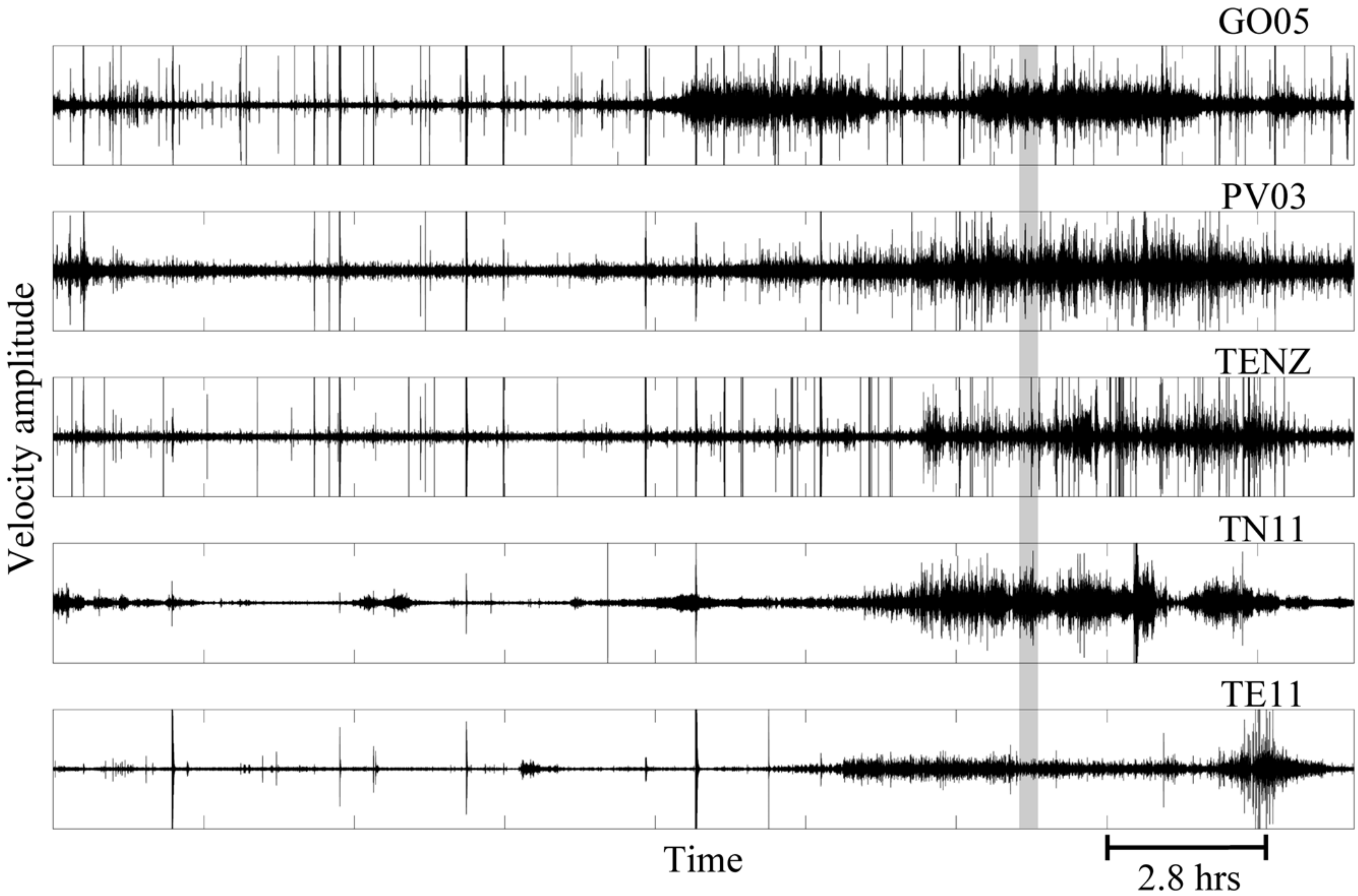

Fig.8

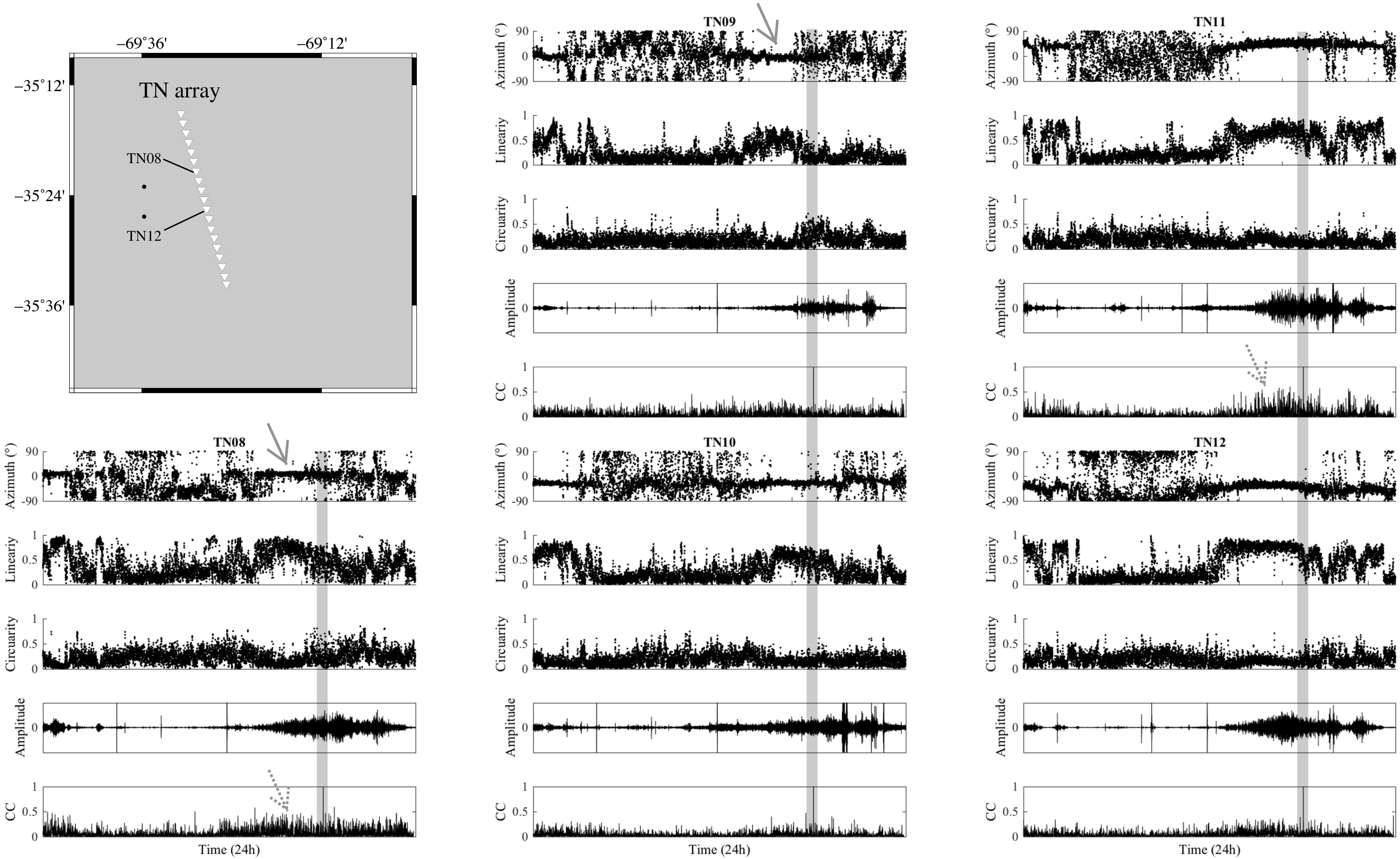

−69°36'
−69°12'
−35°12'
−35°24'
−35°36'
TN array
TN08
TN12
TN09
TN11
TN08
TN10
TN12
Azimuth (°)
Lineary
Circuarity
Amplitude
CC
Time (24h)

Fig.9a

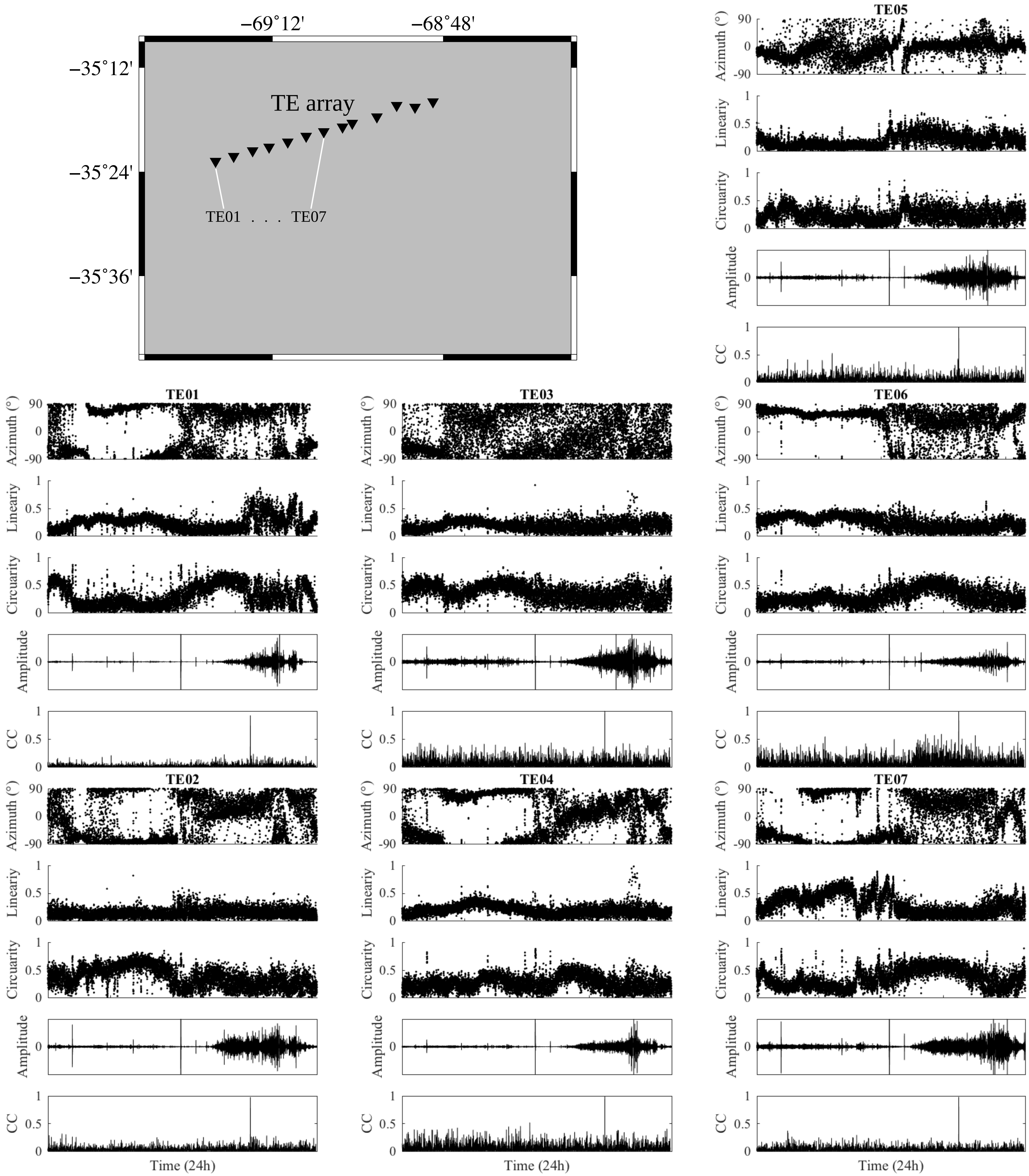
−69°12'
−68°48'
−35°12'
−35°24'
−35°36'
TE array
TE01 . . . TE07
TE05
TE01
TE03
TE06
TE02
TE04
TE07
Azimuth (°)
Linearity
Circuarity
Amplitude
CC
Time (24h)

Fig.9b

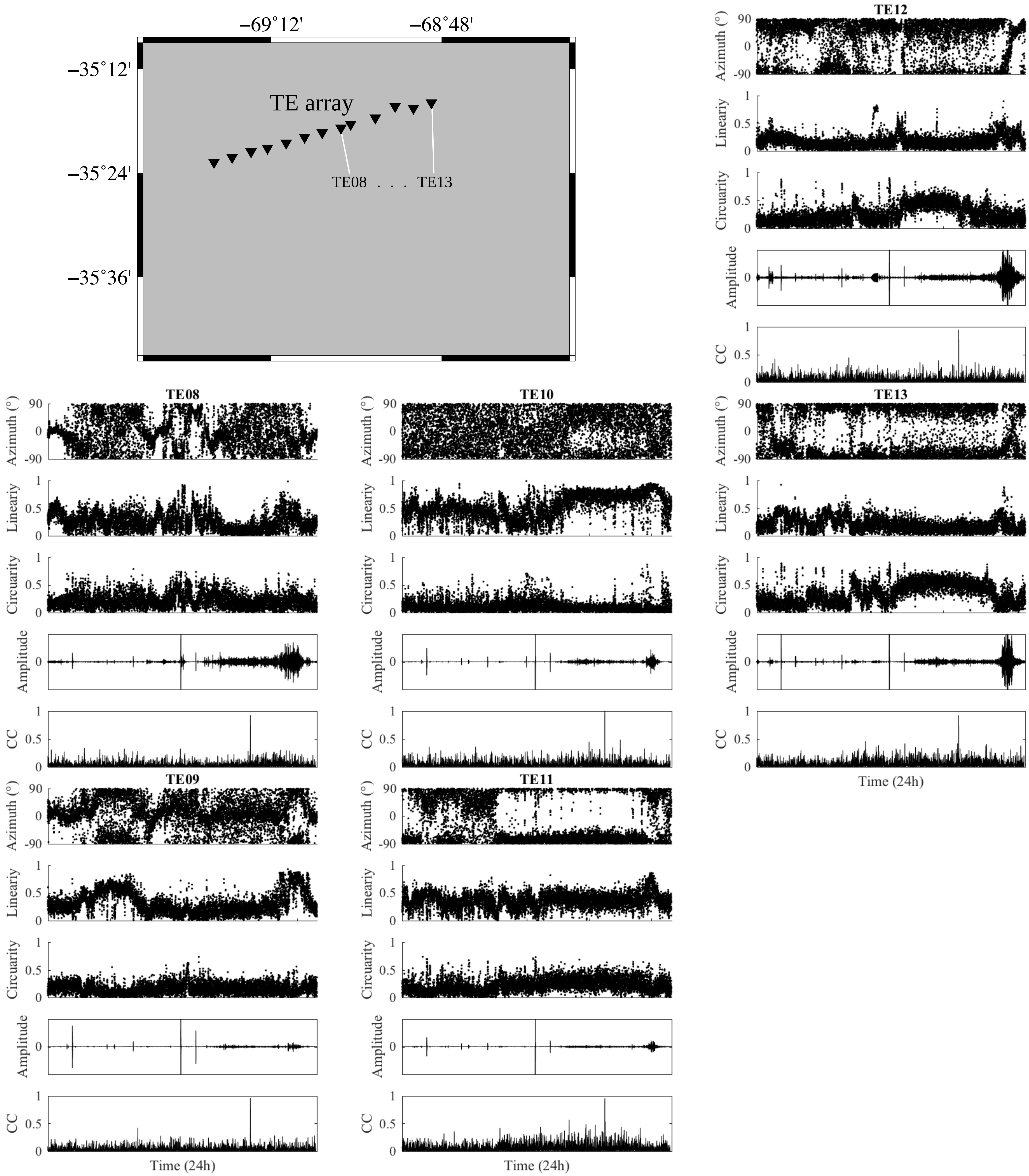
−69°12'
−68°48'
−35°12'
−35°24'
−35°36'
TE array
TE08 . . . TE13
TE08
TE09
TE10
TE11
TE12
TE13
Azimuth (°)
Linearity
Circuarity
Amplitude
CC
Time (24h)

Fig.10

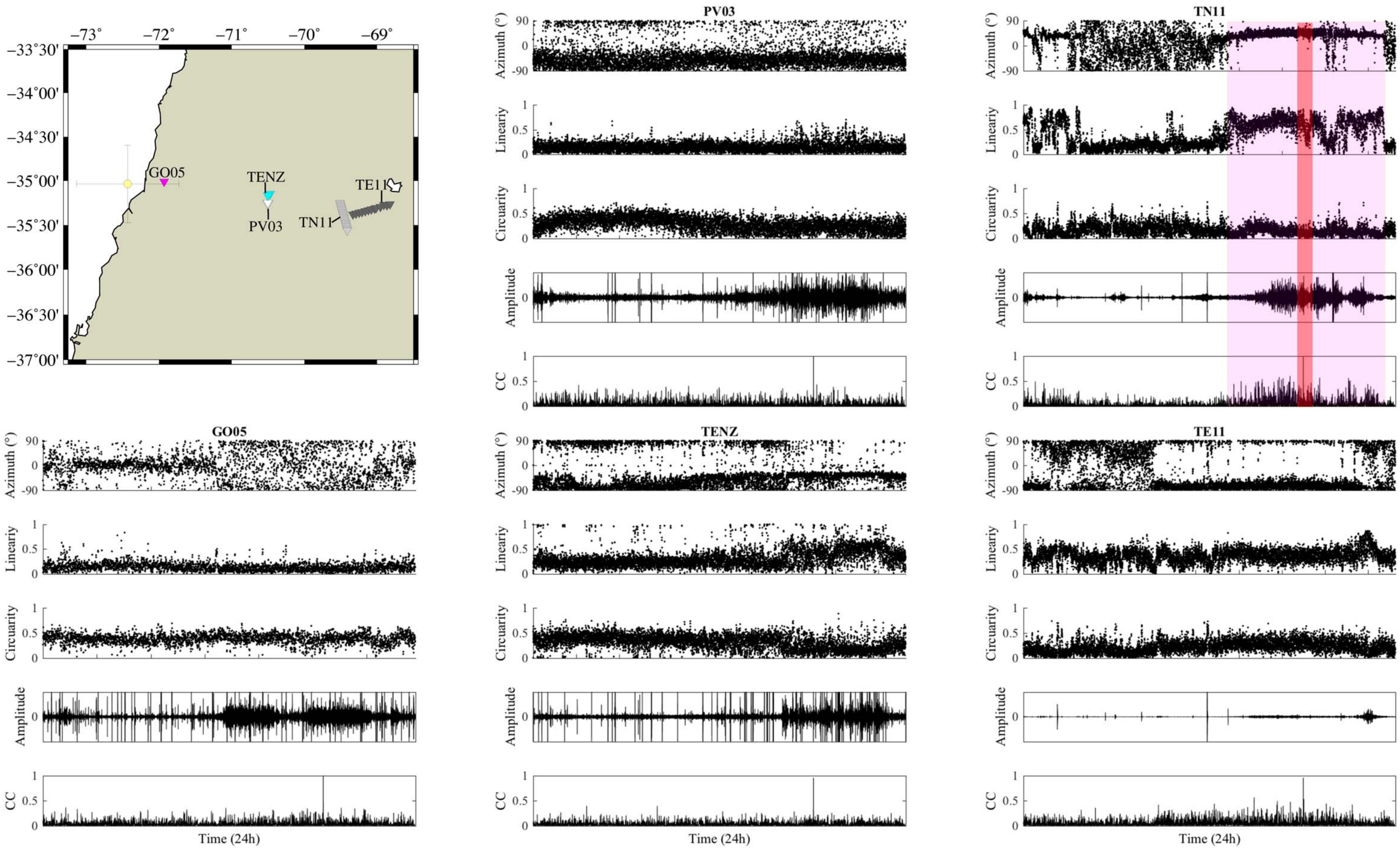

−73°
−72°
−71°
−70°
−69°
−33°30'
−34°00'
−34°30'
−35°00'
−35°30'
−36°00'
−36°30'
−37°00'
GO05
TENZ
PV03
TN11
TE11
PV03
TN11
GO05
TENZ
TE11
Azimuth (°)
Lineary
Circuarity
Amplitude
CC
Time (24h)

Fig.S1

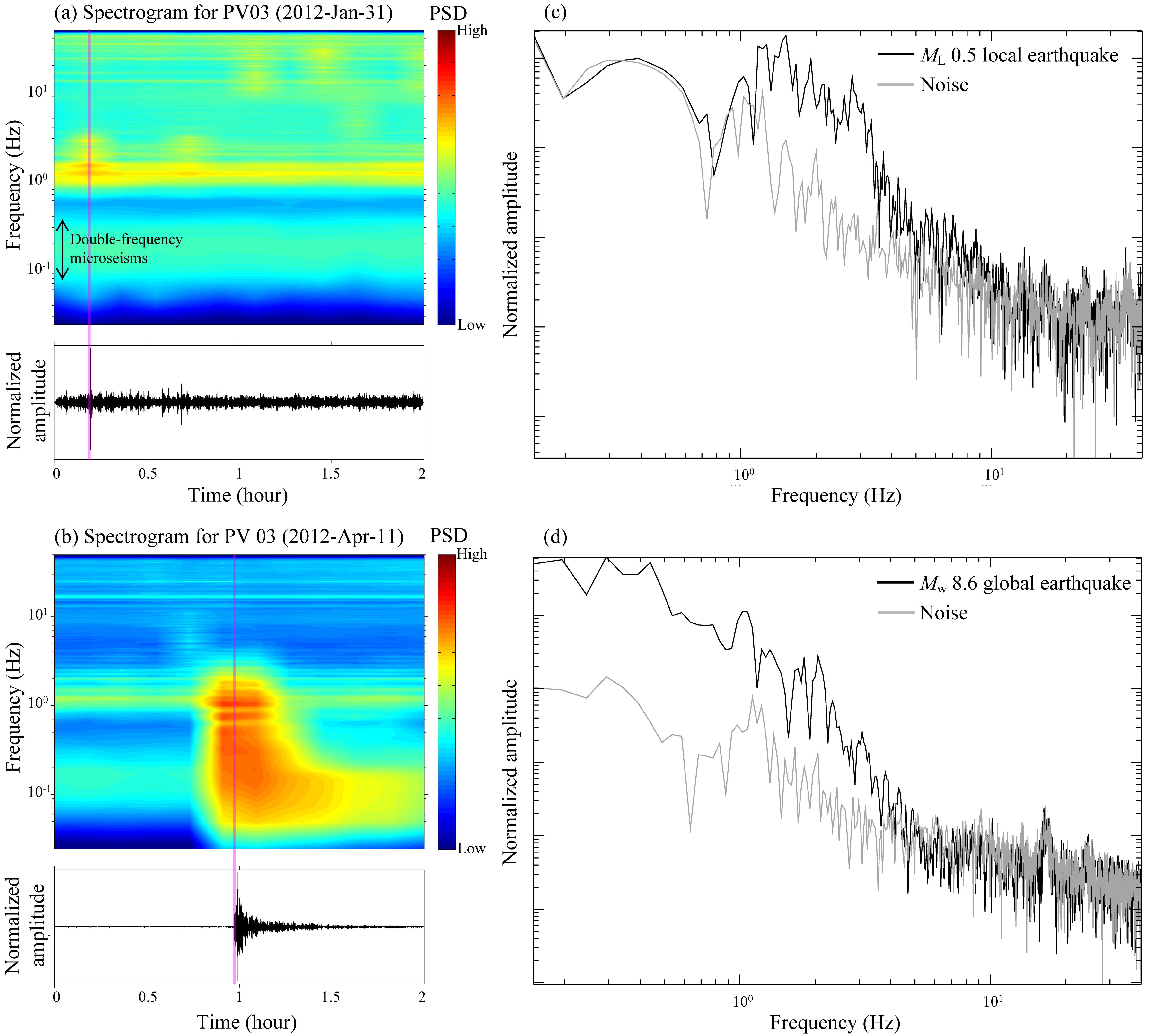
(a) Spectrogram for PV03 (2012-Jan-31)
PSD
High
Low
Frequency (Hz)
10^1
10^0
10^{-1}
Double-frequency
microseisms
Normalized amplitude
0
0.5
1
1.5
2
Time (hour)
(b) Spectrogram for PV 03 (2012-Apr-11)
(c)
M_L 0.5 local earthquake
Noise
Normalized amplitude
Frequency (Hz)
(d)
M_w 8.6 global earthquake

Fig.S2

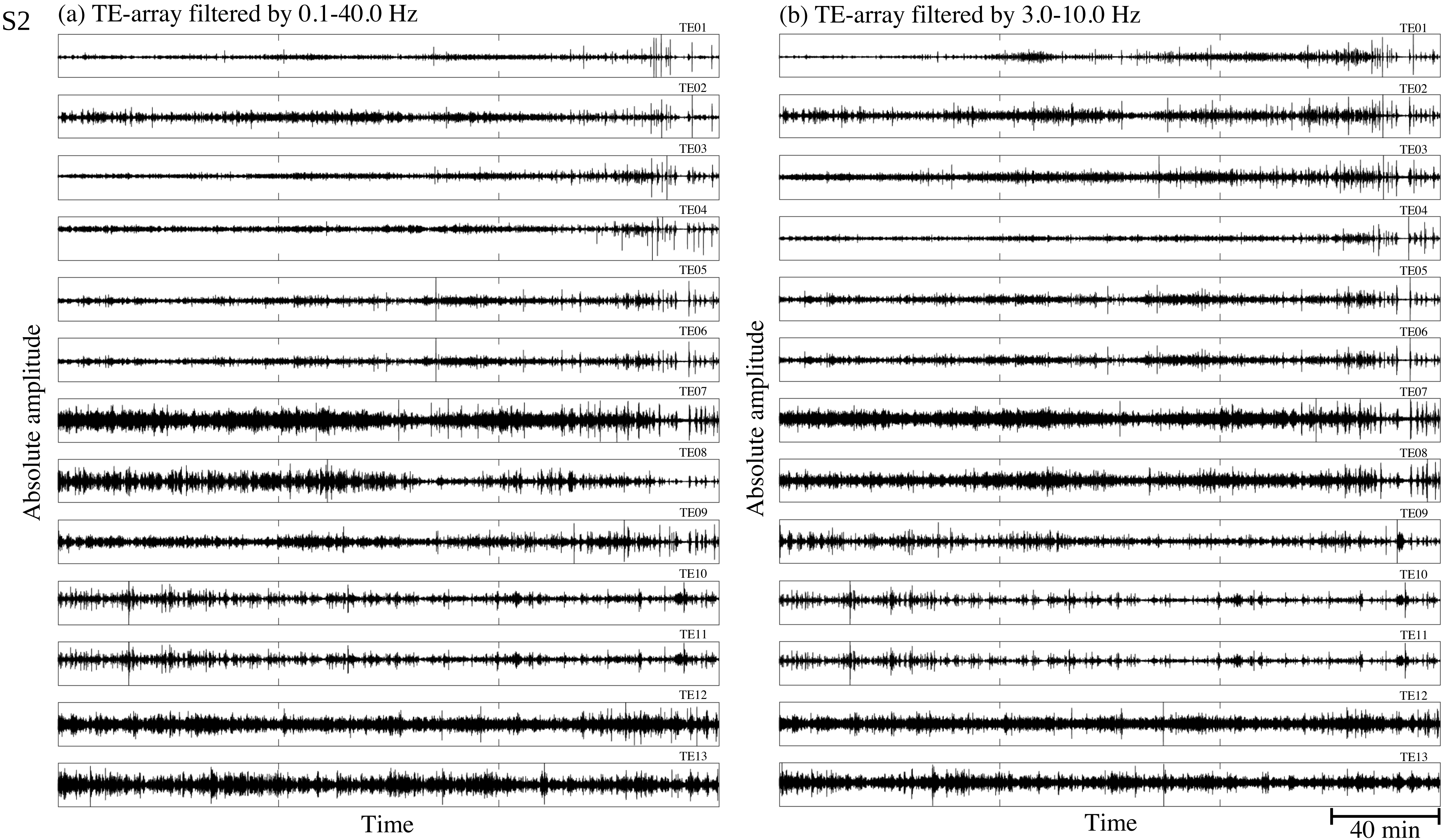
(a) TE-array filtered by 0.1-40.0 Hz
(b) TE-array filtered by 3.0-10.0 Hz
TE01
TE02
TE03
TE04
TE05
TE06
TE07
TE08
TE09
TE10
TE11
TE12
TE13
Absolute amplitude
Time
40 min

TE13

Fig.S3

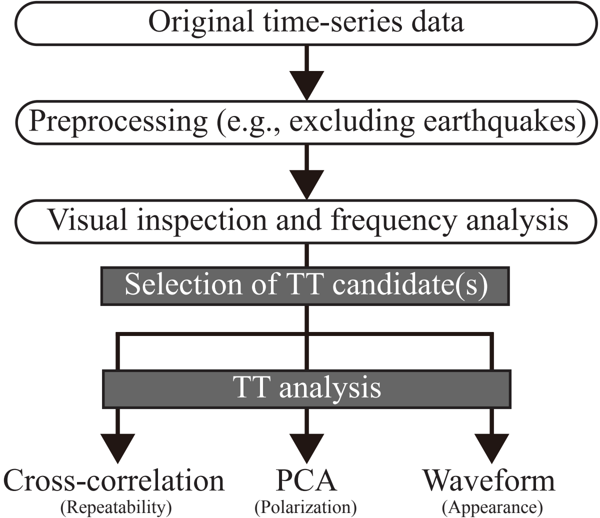
Original time-series data
Preprocessing (e.g., excluding earthquakes)
Visual inspection and frequency analysis
Selection of TT candidate(s)
TT analysis
Cross-correlation
(Repeatability)
PCA
(Polarization)
Waveform
(Appearance)

Fig.S4

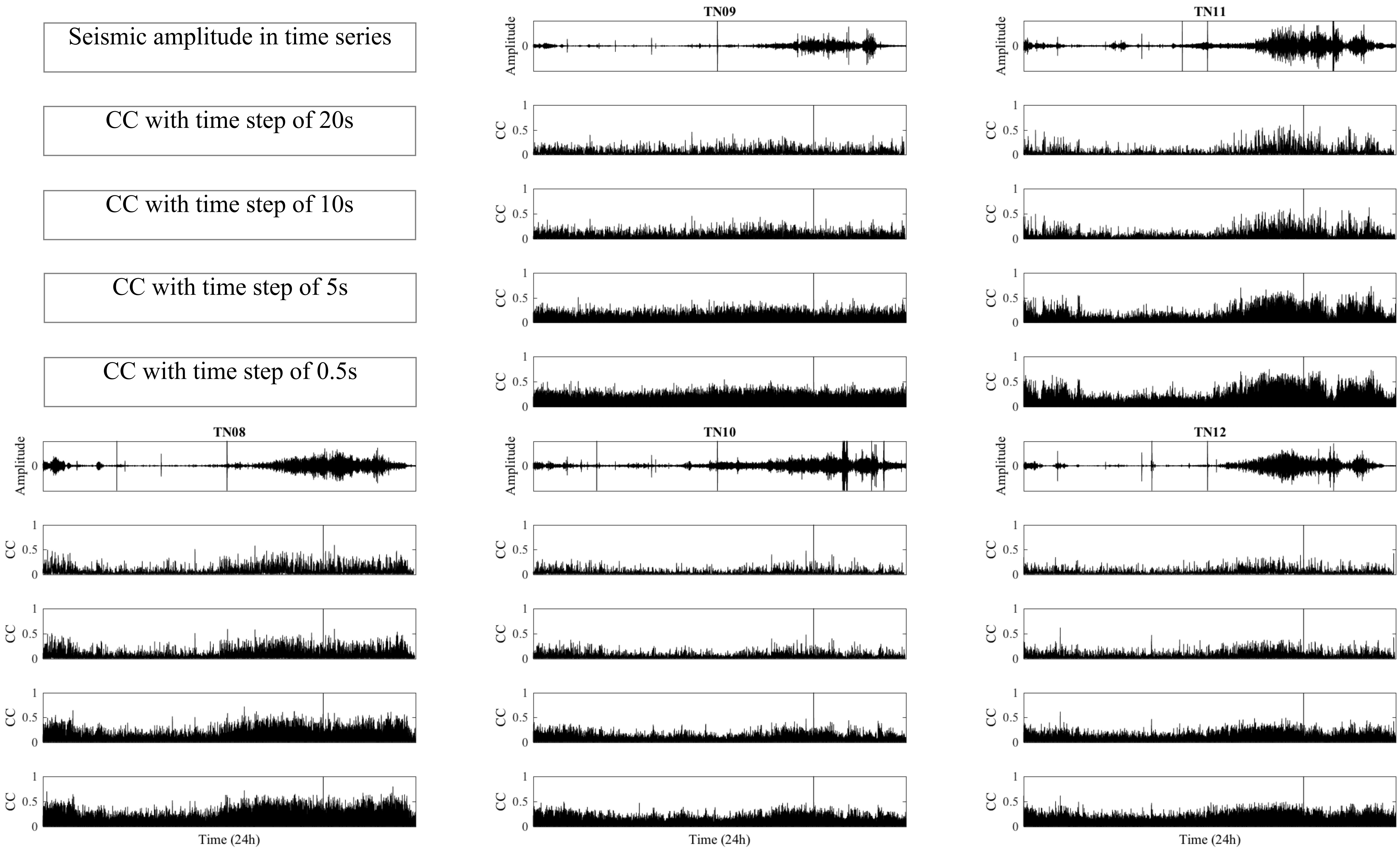

Seismic amplitude in time series
CC with time step of 20s
CC with time step of 10s
CC with time step of 5s
CC with time step of 0.5s
TN08
TN09
TN10
TN11
TN12
Amplitude
CC
Time (24h)

Fig.S5

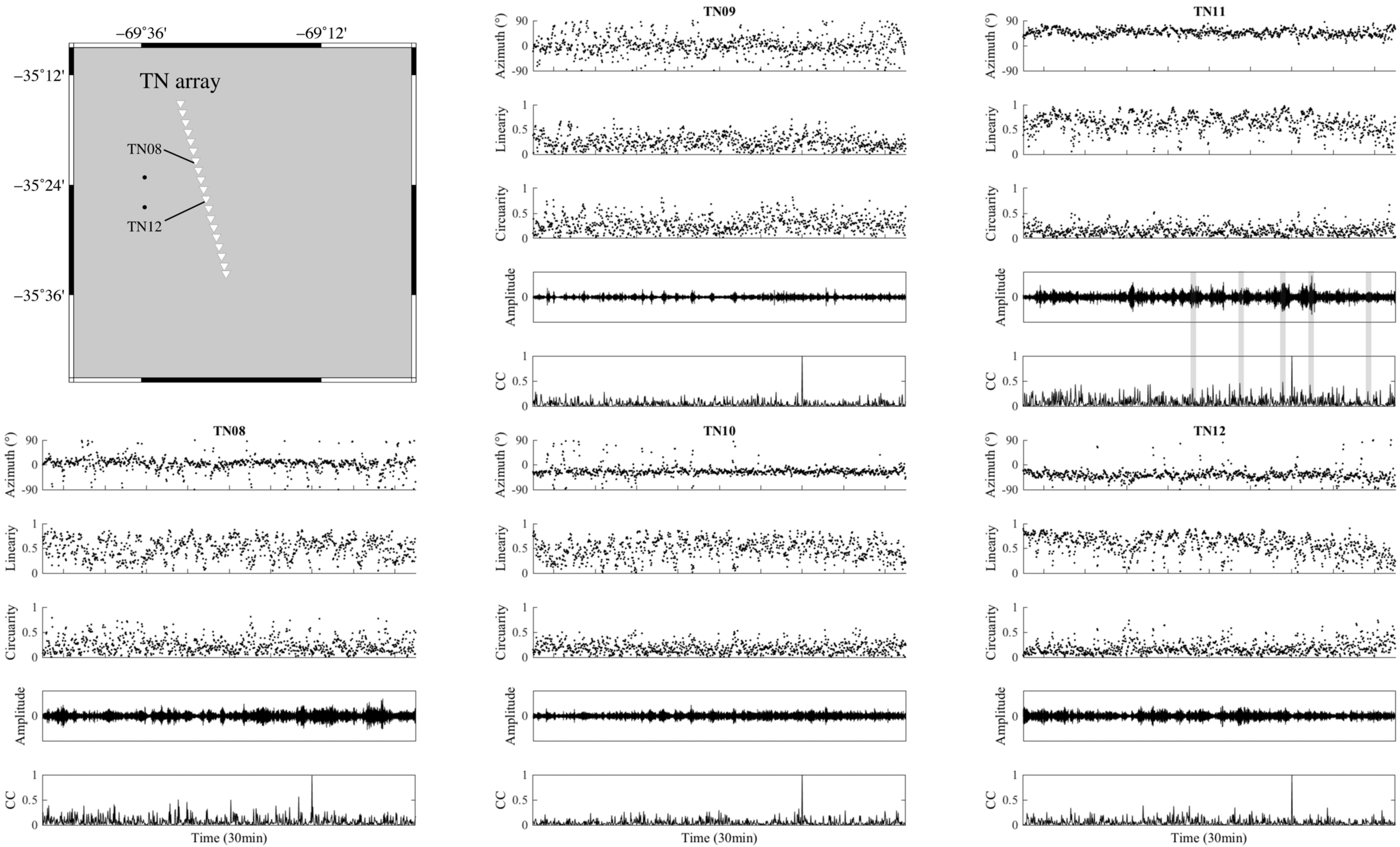
TN array
TN08
TN12
−69°36'
−69°12'
−35°12'
−35°24'
−35°36'
TN09
TN11
TN08
TN10
TN12
Azimuth (°)
Lineary
Circuarity
Amplitude
CC
Time (30min)

Fig.S6

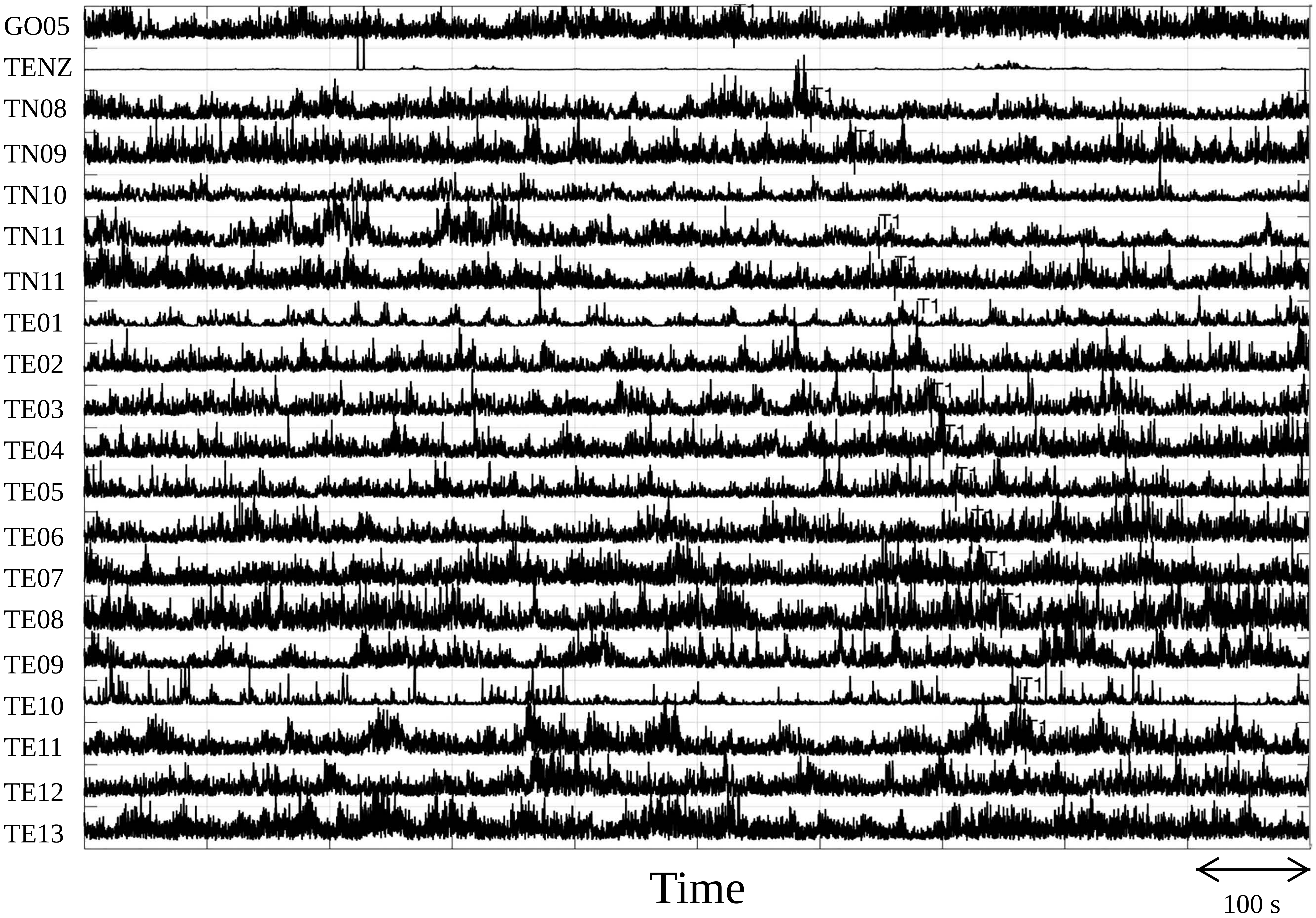

GO05
TENZ
TN08
TN09
TN10
TN11
TN11
TE01
TE02
TE03
TE04
TE05
TE06
TE07
TE08
TE09
TE10
TE11
TE12
TE13
T1
Time
100 s